MASTER

# COMPARISON OF NUMERICAL RESULTS WITH EXPERIMENTAL DATA FOR SINGLE-PHASE NATURAL CONVECTION IN AN EXPERIMENTAL SODIUM LOOP*

Submitted for presentation at Specialists' Meeting on Decay Heat Removal by Natural Convection in FBRs, February 28–29, 1979, Upton, Long Island, N.Y., USA

R. J. Ribando



OAK RIDGE NATIONAL LABORATORY
Oak Ridge, Tennessee 37830

Now at: University of Virginia
Charlottesville, VA



*Research sponsored by the Division of Reactor Research and Technology, U.S. Department of Energy under contract W-7405-eng-26 with the Union Carbide Corporation.

ABSTRACT

A comparison is made between computed results and experimental data for a single-phase natural convection test in an experimental sodium loop. The test was conducted in the Thermal-Hydraulic Out-of-Reactor Safety (THORS) facility, an engineering-scale high temperature sodium loop at the Oak Ridge National Laboratory (ORNL) used for thermal-hydraulic testing of simulated Liquid Metal Fast Breeder Reactor (LMFBR) subassemblies at normal and off-normal operating conditions. Heat generation in the 19 pin assembly during the test was typical of decay heat levels. The test chosen for analysis in this paper was one of seven natural convection runs conducted in the facility using a variety of initial conditions and testing parameters. Specifically, in this test the bypass line was open to simulate a parallel heated assembly and the test was begun with a pump coastdown from a small initial forced flow. The computer program used to analyze the test, LONAC (LOw flow and NAtural Convection) is an ORNL-developed, fast-running, one-dimensional, single-phase, finite-difference model used for simulating forced and free convection transients in the THORS loop. In addition to simulating this particular run, the code has been used to predict results for other runs and for some hypothetical cases involving higher heat generation rates, less heat transfer through the test section walls, etc.

Comparison of LONAC results with experimental data shows fairly good agreement early in the transient, but shows the need for better thermal models of the heat dump, pump and other loop components if long transients are to be simulated. While the THORS loop is only

mildly prototypical of an LMFBR primary loop, this work has provided some insights into the problem of confirming natural convection as a viable means of removing decay heat in the event of loss of forced flow in a loop-type LMFBR.

# 1. INTRODUCTION

At full-power conditions, buoyancy is of little importance to the operation of Liquid Metal Fast Breeder Reactors (LMFBRs). Under decay heat conditions, however, buoyancy will increase the flow over what would be produced by pump motor operation alone. In fact, in current designs buoyancy-driven flow should cool a shutdown reactor enough to give a sufficient margin of safety in the unlikely event of a complete loss of forced flow. A state-of-the-art review of work in the area of natural convection in loop-type LMFBRs in general and in the Fast Flux Test Facility (FFTF) in particular has been given by Addition and Parziale.[1] Singer et al.[2] have made an analogous review for pool-type reactors.

Since no loop-type reactors are presently operating in the United States and loop natural convection data are extremely scarce, most current work is aimed at analytically and experimentally verifying numerical models of components used in system codes such as DEMO[3] for predicting plant operation when making the transition to and operating in the natural convection mode.[4] The test discussed and analyzed in this paper was selected from a series of seven which were conducted in the Thermal-Hydraulic Out-of-Reactor Safety (THORS) facility at the Oak Ridge National Laboratory (ORNL). This loop is used for thermal-hydraulic testing of simulated LMFBR subassemblies at normal and off-normal operating conditions. While not considered a valid surrogate for a reactor primary loop, a comparison of THORS data has been made with results obtained using LONAC (LOw flow and NAtural Convection),[5] an ORNL-developed one-dimensional system-type, single-phase, finite-difference numerical model used for simulating THORS

operation. The exercise has given valuable insights into the pr... of establishing natural convection as a viable means of removing de... heat in the event of loss of forced flow in a loop-type LMFBR.

# 2. DESCRIPTION

## 2.1 Test Facility

The test discussed in this paper was conducted in the THORS [formerly the Fuel Failure Mockup (FFM)] facility. An isometric drawing of primary piping and major components as they were at the time of the test is given in Fig. 2.1. Forced flow is provided by a dc-motor-driven vertical-shaft centrifugal pump capable of delivering 40 liters/sec (600 gpm) at a pressure difference of 960 kPa (140 psi). Heat generation in the simulated LMFBR subassemblies is provided by electrically heated fuel pin simulator (FPS) units. Pressure transmitters, flow meters, and thermocouples are installed to measure the system operating parameters. Electrical trace heaters are installed on all system lines to preheat the system and minimize heat losses during operation.

A test-section inlet valve is available for simulating the pressure drop of the reactor inlet flow paths but was kept fully open in this test. A bypass line with a control valve which can be adjusted to give hydrodynamic simulation of other assemblies in a reactor core is in parallel with the test section. The hot sodium from the test section and sodium from the bypass line mix in the expansion tank. The expansion tank and the piping to it were designed to simulate the hydraulic characteristics downstream of a reactor core, and the expansion tank serves to mix hot and cold sodium, thus protecting the remainder of the loop from excessive temperatures. The ratio of bypass cross-sectional area to that in the test section is approximately

13:1. Programmable power control and pump-speed control capabilities are provided so that prescribed and reproducible flow and/or power transients can be performed.

The pressure of the cover gas above the free surface in the pump bowl is normally regulated at a fixed level [34 kPa (5 psig)]. The pressure of the cover gas above the free surface in the expansion tank may be either fixed at the same level (by opening the cover gas equalizing valve HV-256) or allowed to float (HV-256 closed).

## 2.2 Bundle Description

The test section (referred to as Bundle 6A in this discussion) is a full-length simulated LMFBR fuel subassembly. It consists of 19 electrically-heated pins 5.84 mm (0.230 in.) in diameter spaced by 1.42-mm-diam (0.056-in.) helical wire-wrap spacers on a 305.-mm (12.0-in.) helical pitch. The gap between the bundle and its containing hexcan is 0.71 mm (0.028 in.), one-half the nominal pin-to-pin spacing. This configuration is used to flatten the sodium temperature across the bundle. In order to give a better simulation of the central region of a full reactor subassembly, appreciable effort was expended in designing and fabricating a low thermal inertia bundle housing. The bundle hexcan is 0.51 mm (0.020 in.) thick type 316 stainless steel backed by ~20 mm (~1 in.) of calcium silicate block insulation contained in a stainless steel jacket (Fig. 2.2). Early tests, however, indicated higher values for hexcan thermal inertia than expected and a post-test examination revealed that sodium had

indeed permeated the insulation region. The impact of this sodium leakage on the tests will be discussed later.

The heated length of bundle 6A is .9 m (36.0 in.) with variable-pitch heater windings to produce a 1.5 axial peak-to-mean chopped-cosine power distribution. Downstream of the heated length, a nickel reflector and a simulated fission gas plenum have the same length and thermal inertia as an FFTF fuel assembly. Axial dimensions of the bundle are shown in Fig. 2.3.

Both the heated length and the simulated fission gas plenum are instrumented with wire-wrap thermocouples and duct-wall thermocouples. In addition, the heated length is instrumented with heater-internal thermocouples. The installation of heater-internal and wire-wrap thermocouples is indicated in Fig. 2.4. Duct-wall thermocouples are inserted into holes bored to within 0.121-0.25 mm (0.005-0.010 in.) of the inside surface of the hexcan. At the time of the tests discussed here, there were approximately 45 duct-wall, 33 wire-wrap, and 43 heater internal thermocouples operating reliably in the bundle. Approximately 27 additional thermocouples were strapped to loop piping. Data from these thermocouples and other instrumentation was recorded using a fast response Data Acquisition System (DAS) controlled by a PDP-8E computer. Other details of the THORS DAS may be found in Ref. 6.

## 2.3 Test Procedure

In addition to the test discussed in this paper (referred to hereafter as Test 39), there were one preliminary test and six other natural convection tests run in this phase of the Bundle 6A test

series. Earlier single-phase steady-state forced flow tests run as part of the Bundle 6A test program are reported in Ref. 7; later transient boiling tests are reported in Ref. 8. In the preliminary test, loop trace heater settings were determined so as to minimize heat losses from the system in the temperature range of interest. The other six natural convection tests involved changes in the initial conditions (whether a low forced flow or a zero flow), trace heater settings, the state of the cover gas equalization valve, and power skew in the bundle. Details of the other tests may be found in Ref. 9.

Test 39, the one to be analyzed here in some detail, was the only test in which the bypass leg was open to simulate a parallel bundle. Under isothermal conditions the valve in the bypass was placed at a setting which was thought to give approximately equal pressure drops in the test section and bypass for equal flows, and then the pump speed was adjusted to give about .13 liters/sec (2 gpm) through the test section. The pressure drop coefficient for this valve setting had been measured earlier at higher flows but existing instrumentation was not sensitive enough to make this measurement in the flow range of interest. As in all runs the test section inlet valve was full open. The bundle power was set to 7.3 kW total, while the trace heaters in the bypass leg were set at their maximum output (6.6 kW) to simulate a parallel heated assembly. Once temperatures had stabilized, the pump was stopped and the cover gas equalization valve (HV-256) was opened to begin the test. Approximately two hours later the test was concluded.

## 3. EXPERIMENTAL RESULTS

Plots have been made of the temperature trace in the test section (Fig. 3.1) during the early part of the transient and of the temperature trace around the loop at various times during the whole transient (Fig. 3.2). The abscissa in both plots is distance along the loop in meters measured from the start of the heated section. Data in the test section are from wire-wrap (WW) or heater-internal (HI) thermocouples near the center of the bundle (i.e., thermocouples on pins 1–7). No WW thermocouples were installed upstream of 0.53 m. Data from the rest of the loop are from thermocouples strapped to the outside of loop piping except for two thermocouples that are in wells inserted into the pipes at the test section inlet and outlet. Plots showing the response of selected individual thermocouples as a function of time have been made, but will be discussed later when they are compared to numerical predictions. Data from flowmeters will not be presented because of strong reservations about their validity at such low flows. Experimental heat balances using the indicated flow, temperature increase across the test section, and the bundle power were made throughout the transient. Those made toward the end of the run, when transient heat storage effects in the bundle should be at a minimum, suggest flow meters generally reading some 50–80% high. The quoted accuracy of the flowmeters is about ±70% of the flow predicted by the LONAC code for this case.

Since Test 39 began with a pump coast down from approximately 0.13 liters/sec (2 gpm, 5% nominal flow) peak temperatures initially are

recorded toward the end of the heated section (Fig. 3.1). During a transitional period between $\tau$ = 100 and $\tau$ = 150 sec, the peak temperature is found nearer the bundle midpoint where the heat generation is at its maximum. Finally after a substantial natural convection flow has been set up, the peak again is recorded toward the end of the heated section. Other phenomena appearing in the plot of loop thermocouples vs time (Fig. 3.2) is the very large thermal inertia of the expansion tank as evidenced by the delay in the response of the thermocouple just downstream of it. It is also readily apparent that the very large heat loss in the area of the heat dump affects the inlet thermocouple as well as the one at the outlet.

# 4. ANALYSIS

## 4.1 Procedure

Analysis of the bundle 6A natural convection tests has been based on use of LONAC,[5] a one dimensional, single phase, finite-difference model for predicting THORS transients. The early version of this code had no provision for thermal inertia of piping and loop components such as the pipe [illegible] included no heat losses. Inclusion of structure thermal [illegible] piping losses and a fairly detailed model for the insulation and containment around the test bundle itself was essential to the simulation of the Bundle 6A tests. As noted earlier, sodium had permeated the insulation surrounding the test bundle and the resulting heat sink had to be fairly carefully modeled since it was in such close proximity to the pin bundle. Other structural components such as piping, the pump, expansion tank, and heat exchanger were thermally modeled simply as single nodes in intimate contact with the adjacent sodium node (c.f. Ref. 10).

Since a fairly detailed discussion of the LONAC solution algorithm has been given previously,[5] only a few points will be made here. The loop and bundle are divided into 36 energy nodes, 34 of which are of fixed volume. The other two represent the sodium in the pump bowl and expansion tank. The sodium levels in these two nodes are predicted by the code. Accurate prediction of these levels is particularly important because, for example, in the case of the pipe run between the expansion tank and pump bowl, the temperature field in this line normally would tend to drive the flow in the negative

direction were at [illegible] face heights were
in some tests argon pressurization in the [illegible].

LOMAC solves [illegible] equation
equations:

$$A \frac{\partial}{\partial \tau} + \frac{\partial}{\partial Z} \qquad , \tag{1}$$

$$A \frac{\partial(\rho h)}{\partial \tau} + \frac{\partial M_S h_S}{\partial} + \frac{\partial(GhA)}{\partial Z} = \qquad , \tag{2}$$

$$A \frac{\partial G}{\partial \tau} + \frac{\partial}{\partial Z} \frac{G^2 A}{\rho} = -A \frac{\partial p}{\partial Z} - \left(K + \frac{fL}{d}\right) \frac{}{2\rho} - \rho g A \ , \tag{3}$$

where

A = cross-sectional area,

d = hydraulic diameter,

f = friction factor,

G = mass flow/area,

g = gravitational acceleration,

h = enthalpy,

$h_S$ = enthalpy of structure,

K = pressure drop coefficient,

L = length,

$M_S$ = mass of structure,

p = pressure,

Z = coordinate in flow direction,

$\rho$ = density,

$\tau$ = time, and

$\phi$ = heat source term.

A five node fuel pin [illegible] ...tion model is coupled to each sodium node in the heated zone. Similarly a five node radial conduction model for the insulation surrounding the test bundle and [illegible] coupled to all test section axial nodes (both in the heated section and in the simulated fission gas plenum section). Runs were [illegible] using manufacturer's data for the insulation thermal properties and using estimated properties for the sodium-saturated insulation.[8] Other than in the test section, pipe [illegible] other [illegible] ponents were assumed to be at the same temperature as the contiguous sodium. Whereas pipe heat capacity is less than half that of the contained sodium for the large pipes used in a full scale reactor,[12] pipe heat capacity ranges from 80 to 120% of the sodium in the small diameter pipes in THORS. The estimated or calculated masses of other loop components which were included in the thermal analysis were: heat dump (but not its support structure), 279 kg; expansion tank, 261 kg; top and bottom flanges of test section, 45 kg; and pump (impeller and bowl only), 241 kg.

Losses from loop piping and other components were estimated using the results of the preliminary test mentioned earlier. An analytical determination of the heat losses would have been difficult if not impossible because of the large number of protuberances such as valves and flowmeters as well as the irregular geometry of elbows, tees and the pump. A scheme was developed for allocating the trace heat between losses to ambient and gains to the flowing sodium based on a comparison between the computed sodium temperature and the temperature for which the trace heater setting had been made. The resulting additional term in the energy equation for the flowing sodium is:

$$\frac{Q_{el}}{T_{TKS} - T_{\infty}}$$

For Test 39 $T_{TKS}$, the piping temperature corresponding to the trace heater setting, was 480°C (900°F) in the hot leg and 320°C (600°F) in the cold leg. Ambient temperature was about 46°C (115°F). Total trace heat under than in the bypass was about 12.1 kW. This is nearly equal to the combined electrical input to the test section and the heated bypass. Assuming about a 350°C (660°F) hot leg temperature early in the transient, about 1/3 of the trace heat in the hot leg would flow into the sodium; later the fraction would be about 1/10. The cold leg does not deviate much from the 320°C (600°F) temperature; therefore, the additional heat input due to the trace heat would be small. Other details on the scheme for allocating the trace heat may be found in Ref. 9.

The momentum equations are set up using the momentum integral method discussed by Meyer.[13] Momentum nodes are set up in a staggered arrangement so that mass flows are computed at the edges of the mass/energy nodes rather than at their centers where thermodynamic properties (density and energy) are defined. Frictional losses, thermal heads, etc., are computed locally at each momentum node. Since the flow through a line at any point may be expressed in terms of the flow at the inlet to that line plus a correction because of thermal expansion or contraction up to that point, it is possible to combine the momentum equations for a series of nodes into one equation for the whole string. When the bypass line is open, four separate momentum equations result: one each for the main line from the pump to the

tee, the bypass line from the tee to the expansion tank, the test section line from the [illegible] the expansion tank and the main line from the expansion tank back through the heat dump to the pump bowl. These equations are algebraically manipulated to eliminate the pressure at the tee. The [illegible] profiles for transient flow redistribution because of different thermal heads in the bypass and the test section. For other tests with the bypass line closed, there are basically only two momentum equations to be solved. [illegible] Engel[9] were used for laminar and transition friction factors in the pin bundle. The stopped-rotor pressure drop of the pump was assumed to be neglible.

## 4.2 Results

A LONAC simulation of Test 39 was made using the estimated degraded test section insulation thermal properties. In addition, simulations were made using the Test 39 procedure with both degraded and "as built" insulation properties and at several bundle powers in addition to the actual one. Simulations of several other tests were made and are discussed in Ref. 9. Weighted averages of the nearest experimentally measured temperatures were used to determine initial temperatures for each of the finite-difference volumes. Since the argon cover gas in the expansion tank was pressured at $\tau \leq 0$, it was assumed that when the two free surfaces were at the equilibrium no-flow level and the loop was at 320°C (600°F), the cover gas gauge pressure was 34 kPa (5 psig). Pressure changes due to heating or to level changes could then be computed. This calculational procedure

has some basis in the experimental procedure used and was necessitated by the lack of pressure and temperature measuring devices in the cover gas space at the time.

As noted earlier Test 39 was the only run in which the bypass line was open to simulate a parallel heated assembly. The pressure drop coefficient, determined as noted on Sect. 2.3, was used for the bypass line valve in the simulation; and, under isothermal conditions, the pump head was iterated until the desired 0.13 liters/sec (2 gpm) flow was obtained in the test section. The corresponding computed flow in the bypass was about 2.4 times this rather being equal as desired. Trace heat in the bypass was set at its maximum value ( 6.6 kW).

Computed temperatures in the test section and around the loop and flows are shown in Figs. 4.1, 4.2, and 4.3. Figures 4.1 and 4.2 may be compared to Figs. 3.1 and 3.2 which show the corresponding experimental data. The circled numbers on Fig. 4.2 show the time it would take a parcel of fluid leaving the beginning of the test section at $\tau = 0$ to reach the station indicated. From the expansion tank downstream the flow is, of course, augmented by the bypass flow. The computed flows (Fig. 4.3) for this run are particularly interesting because the experimental procedure involved a simultaneous pump coastdown and expansion tank cover gas depressurization. The effects are particularly apparent in the lightly damped flow oscillation through the heat dump.

Individual thermocouple traces and corresponding LONAC results have been plotted as a function of time for a number of positions around the loop. These are depicted in Figs. 4.4 through 4.7. In most cases the center of the LONAC node did not fall at a thermocouple

position. Hence the value indicated as "LONAC Prediction" is the node nearest the thermocouple and does not reflect any weighting. Thermocouple identification numbers are keyed to the loop diagram (Fig. 2.1). It may be seen that LONAC has overpredicted temperatures within the heated section (location 1) and at the end of the heated section (location 2). The peak temperature predicted by LONAC was 462°C at 690 sec vs the 448°C observed in the loop at about 600 sec. At a representative point in the simulated flow plenum (location 3) the comparison is somewhat better. At location 4, which is commonly referred to a "test section outlet" is actually much closer to the [illegible] inlet, the prototype is seen to respond more sluggishly than the prediction. It must be noted that the heat capacity of the hardware in this area, most notably the flow meter, was not included in this simulation and could account for the difference.

At the next location (4, expansion tank outlet) LONAC first overpredicts and after about 3000 sec underpredicts. It is highly likely that the discrepancy is caused by the fact that the fluid in the expansion tank is thermally stratified, while in the one node LONAC representation, it is assumed to be well-mixed. For this reason the LONAC outlet value is representative of the mean rather than of the temperature at the bottom of the tank. The characteristic thermal diffusion time computed for a layer of sodium of thickness equal to the free surface height in the expansion tank is about 900 seconds. This is virtually the same as the time it would take to flush the expansion tank sodium inventory given the computed test section and bypass line flows. It suggests that insufficient time for thermal

equilibration is allowed and that hot fluid is added to the top while cold fluid is drawn off the bottom.

Location 6 has been chosen some distance upstream from the heat dump because the thermocouple just at the inlet reflects the huge losses in the heat dump and its vicinity rather than being representative of the incoming fluid. In other words the losses at the heat dump are really not confined to the dump per se while in the LONAC simulation they are. With this proviso the LONAC results are reasonable although the effect of the stratification in the expansion tank may still be seen.

Locations 7, 8, 9, and 10 show fairly good agreement although it must be pointed out that trace heat in the cold leg of the loop was set to attempt to maintain 600°F (320°C) temperatures throughout the transient. Recorded values did not deviate much from this. In contrast both measured and computed temperatures in the hot leg did vary significantly from the 900°F (480°C) trace heater set point.

The location in the bypass (11 and 12) seems to indicate that the flow in the bypass has been overpredicted somewhat. This is presumably the result of poor characterization of the valve pressure drop coefficient under low flow conditions. The slower transient response seen in both the experimental data and the simulation is directly attributable to the greater sodium inventory in the bypass line as opposed to the test section.

Friction and form losses as well as thermal head for this case are plotted as a function of time in Fig. 4.8. The thermal heads have been computed as $\int \rho g dz$ around the loop with the path taken through the

test section in the one case and through the bypass in the other. Hydraulic losses have been computed separately for the bypass, the test section and the remainder of the loop. Losses in the remainder of the loop are seen to be minimal and, other than at very early times, temperal accelerations is also negligible.

In order to assess the effects of higher bundle power and of insulation integrity on the results, five additional runs were made. These include two runs made using the estimated degraded insulation thermal properties but higher powers (to the bundle only, not the heated bypass). Runs were also made at the three bundle powers but using "as built" insulation thermal properties. The results are summarized in Fig. 4.9 which shows the peak bundle temperature and Fig. 4.10 which shows the time to reach the peak temperature. Note that Fig. 4.10 shows an order of magnitude difference between "as built" and degraded cases. In the former case, temperatures and flows rise quickly and in the case of the flow there is even an overshoot before it damps out. Test 39 data are seen to compare quite favorably with the degraded insulation results at the same power.

## 5. CONCLUSIONS

As has been seen, fairly good agreement was obtained between experimentally measured and LOOP-predicted peak temperatures. The temperature profiles early in the transient were also fairly well-matched by the code. Some reasons for this success and other observations will be discussed in this section.

In a large-scale reactor the sodium flow on the primary side of the intermediate heat exchanger (IHX) is in the vertical direction and involves a substantial elevation change over the length.[12] In contrast the sodium flow through the THORS Na-air 0.5MW heat dump is in nearly the horizontal direction. Thus the crudeness of the heat dump thermal model is not felt until the thermal pulse reaches a vertical leg. Further refinement of the heat dump model would be difficult because with the blower off and the damper closed, the heat dump was operating at only a few percent of its design rating. As noted earlier trace heaters on the heat dump tubes and supplementary radiator heaters were off during these tests. A more sophisticated model would also have to include at least part of the massive heat dump support structure. Sodium flow in the new 2.0 MW heat dump to be used for future THORS tests with larger bundles will be upward rather than downward as in the primary side of a reactor IHX. The 0.5 MW heat dump used in these tests will continue to be available.

For similar reasons the crude pump thermal model does not affect the early part of the transient. Future THORS natural convection tests would involve a new electromagnetic (EM) pump which will be located in a vertical piping leg. When not operating, the EM pump may

be characterized hydraulically as simply another length of straight pipe. Its thermal behavior should be somewhat [illegible] characterize than that [illegible] centrifugal pump.

As illustrated [illegible] 4.9 and 4.10, the thermal properties of the insulation surrounding the test bundle play a dominant role in the transient. Manufacturer's [illegible] was available for the "as built" insulation, but the properties of the degraded insulation could only be estimated. The manufacturer's data indicated [illegible] porosity of the material was 53%. Under the assumption that all pore space was full of sodium, a thermal conductivity which was 53% that of pure sodium (and over 200 times that of the "as built" insulation) was used for the degraded insulation. Similarly the heat capacity was computed on the basis of 53% sodium and 47% insulation. Clearly the agreement (or disagreement) between experimental and LONAC values seen in Figs. 4.9 and 4.10 is a strong function of this assumption. In a full-scale reactor the hexcan wall and adjacent subassemblies, if cooler, would have important effects as heat sinks during a slow natural convection transient.

The pressure drops in the bundle and bypass were orders of magnitude larger than that in the rest of the loop. Under the decay heat conditions simulated here the flow in the bundle is in the laminar and transition regimes. This is also the case for the full-scale reactor under decay heat conditions; but in the reactor many more, larger assemblies feed the also larger loop piping. The result is that in THORS the flow in the loop piping is in the laminar and potentially troublesome-to-evaluate transition regimes, while that in reactor piping would be well into the turbulent regime. Again because the bulk

drop is in the bundle where apparently it has been well-model[illegible] al et al. results, the [illegible] appears not to matter. Similarly the neglect of the pump stopped-rotor pressure drop [illegible] not to be a problem in THORS.

The THORS tests discussed in these tests have generated a wealth of loop and intra-assembly data under simulated decay heat conditions. They have demonstrated the ability of a simplified computer code to model the THORS loop, the older segments of which were designed nearly a decade ago with little consideration of detailed loop temperature measurements required for testing under natural convection conditions. The tests and analysis discussed here have given insights which will be helpful in planning future tests under natural convection conditions and insights which will help in code improvements for simulating long transients.

Fig. 2.1. Drawing of the THORS facility for Bundle 6A operation. Circled numbers indicate the position of thermocouples used for comparison of experimental results with numerical predictions in Figs. 4.4 through 4.7.

Fig. 2.2. Cross section of Bundle 6A.

Fig. 2.3. THORS Bundle 6A test-section assembly showing axial dimensions (1 in. = 25.4 mm).

Fig. 2.4. Bundle 6A fuel pin simulator.

Fig. 3.1. Temperatures recorded along the bundle axis plotted at selected times early in the transient, (THORS Bundle 6A, Test 39, initial low forced flow, bypass open).

Fig. 3.2. Temperatures recorded around the THORS loop plotted at selected times during the transient, (THORS Bundle 6A, Test 39, initial low forced flow, bypass open).

Fig. 4.1. Computed test section temperatures for various times early in the transient (LONAC simulation of THORS Bundle 6A, Test 39).

Fig. 4.2. Computed loop temperatures for various times during the transient, (LONAC simulation of THORS Bundle 6A, Test 39). Circled numbers indicate the time (sec) it would take a parcel of fluid leaving the beginning of the heated section at  = 0 to reach the station indicated.

Fig. 4.3. Computed flows vs time (LONAC simulation of THORS Bundle 6A, Test 39).

Fig. 4.4. Comparison of Test 39 thermocouple data with LONAC predictions at stations 1 through 3. Position of stations is indicated in Fig. 2.1.

Fig. 4.5. Comparison of Test 39 thermocouple data with LONAC predictions at stations 4 through 6. Position of stations is indicated in Fig. 2.1.

Fig. 4.6. Comparison of Test 39 thermocouple data with LONAC predictions at stations 7 through 9. Position of stations is indicated in Fig. 2.1.

Fig. 4.7. Comparison of Test 39 thermocouple data with LONAC predictions at stations 10 through 12. Position of stations is indicated in Fig. 2.1.

Fig. 4.8. Computed thermal heads and losses vs time for Test 39.

Fig. 4.9. Peak temperatures [illegible] in Test 39 compared with LONAC predictions for this case and hypothetical cases using the Test 39 procedure.

Fig. 4.10. Time calculated to reach the peak temperatures plotted in Fig. 4.9, (LONAC simulation using Test 39 procedure, both with "as built" and degraded insulation and actual and higher bundle powers). Test 39 value is also plotted.

## REFERENCES


1. S. L. Additon and E. A. Parziale, "Natural Circulation in FFTF, A Loop Type LMFBR," *Symposium on the Thermal and Hydraulic Aspects of Nuclear Reactor Safety*, Vol. 2, Liquid Metal Fast Breeder Reactors, ASME, 1977, p. 265-283.

2. R. M. Singer, D. Grand, and R. Martin, "Natural Circulation Heat Transfer in Pool-Type LMFBR's," *Symposium on the Thermal and Hydraulic Aspects of Nuclear Reactor Safety*, Vol. 2, Liquid Metal Fast Breeder Reactors, ASME, 1977, pp. 233-264.

3. "LMFBR Demonstration Plant Simulation Model (DEMO)," WARD-D-0005, Rev. 4, Jan. 1976.

4. R. D. Coffield et al., *LMFBR Natural Circulation Verification Program (NCVP). Review of Experimental Facilities and Test Recommendations*, WARD-NC-3045-1, July 1977.

5. R. J. Ribando, *LONAC: A Computer Program to Investigate Systems Dynamics Under Conditions of Low Forced Flow and Natural Convection*, ORNL/TM-6228, April 1978.

6. N. E. Clapp, *The Data Management System for the Thermal-Hydraulic Out-of-Reactor Safety Facility Computer Controlled Data Acquisition System Configuration for Bundle 3C Operation*, ORNL/TM-6745, February 1979.

7. J. L. Wantland et al., *Steady-State Sodium Tests in a 19-Pin Full-Length Simulated LMFBR Fuel Assembly -- Record of Steady State Experimental Data for THORS Bundle 3A*, ORNL/TM-6106, March 1978.

8. [illegible] et al., *[illegible]* ANL/RAS-[illegible], January 1979.

9. [illegible] et al., *[illegible]* ANL/FPP-6778, to be published.

10. [illegible] *[illegible]* WAPD-[illegible], [illegible] 1972.

11. [illegible] *[illegible]* WAPD-PT-20, [illegible] pp. 61-72.

12. *[illegible]* [illegible]-77-06.

13. J. E. Meyer and R. P. Rose, "Application of a Momentum Integral [illegible] of Parallel Channel Boiling Oscillations," *Journal of Heat Transfer, Trans. ASME,* Series C, Vol. 85, 1963, pp. 1-9.

14. F. C. Engel, R. A. Markley, and A. A. Bishop, "Laminar, Transition and Turbulent Parallel Flow Pressure Drop Across Wire Wrap Spaced Rod Bundles," *Nuclear Science and Engineering,* Vol. 69, No. 2, February 1979, p. 290.

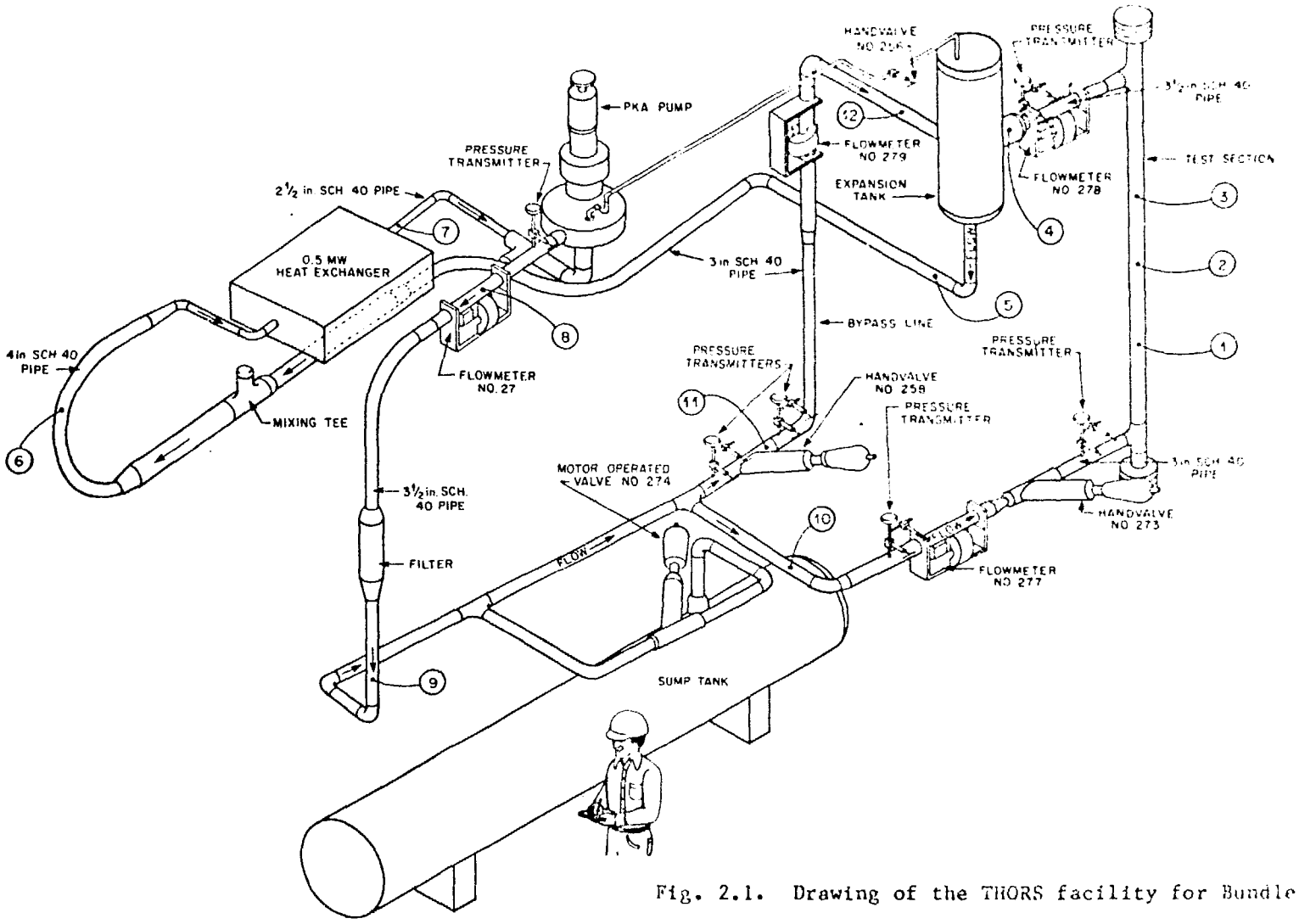


Fig. 2.1. Drawing of the THORS facility for Bundle 6A operation. Circled numbers indicate the position of thermocouples used for comparison of experimental results with numerical predictions in Figs. 4.4 through 4.7.

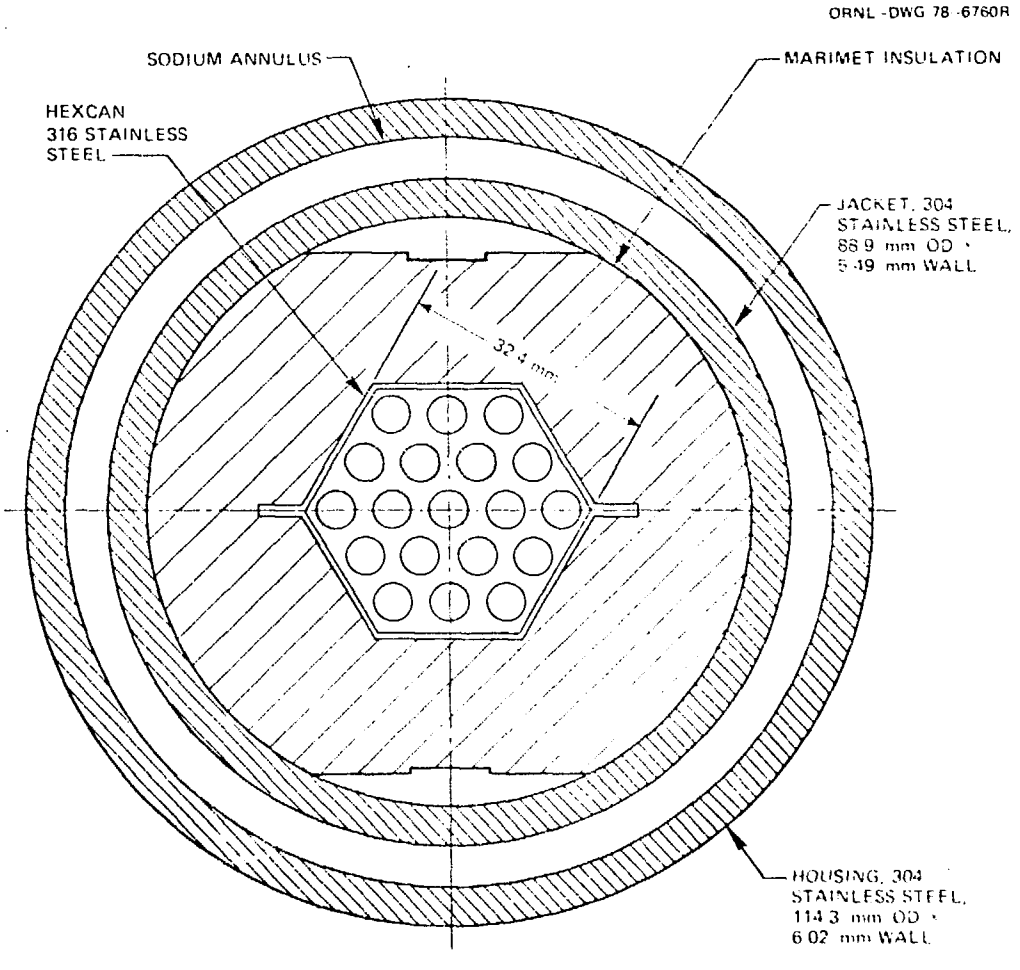


Fig. 2.2. Cross section of Bundle 6A.

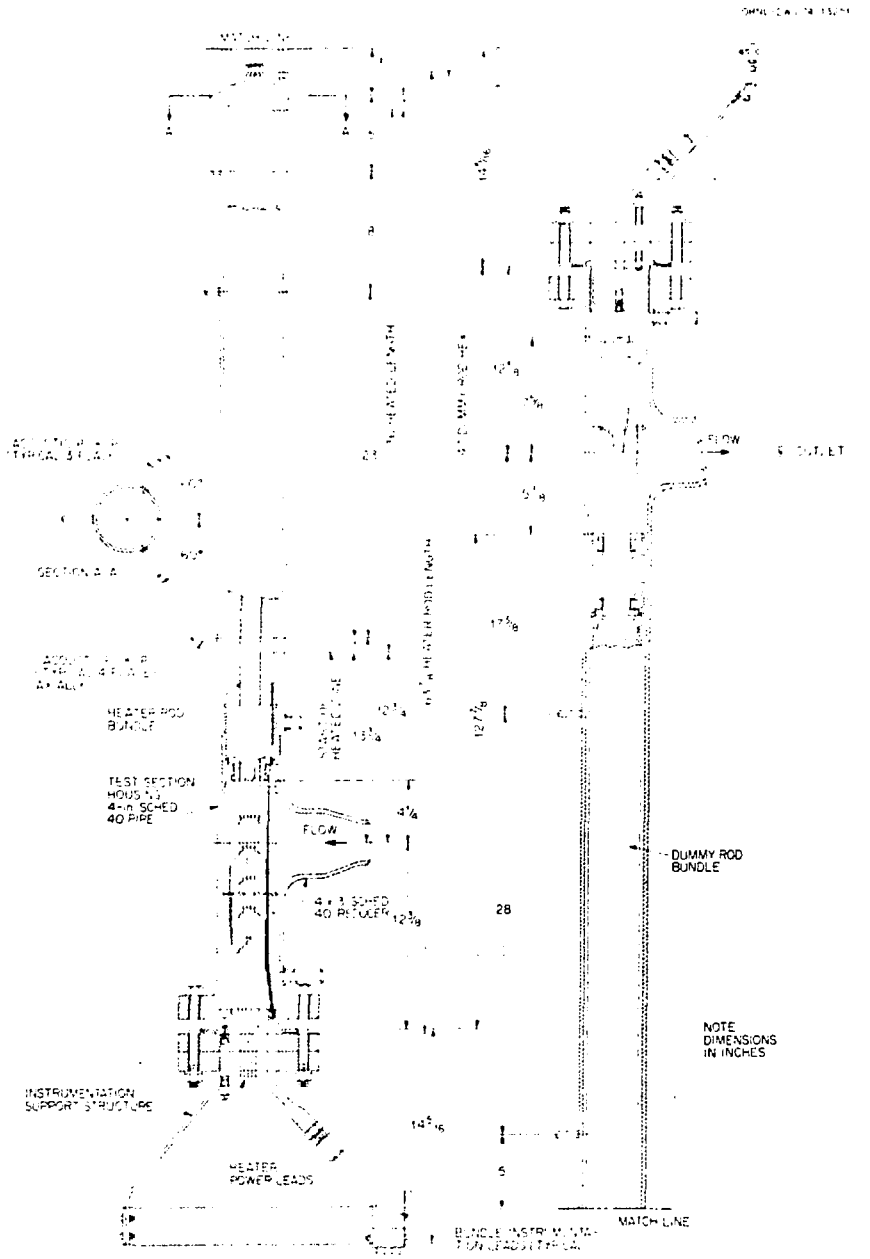


Fig. 2.3. THORS Bundle 6A test-section assembly showing axial dimensions (1 in. = 25.4 mm).

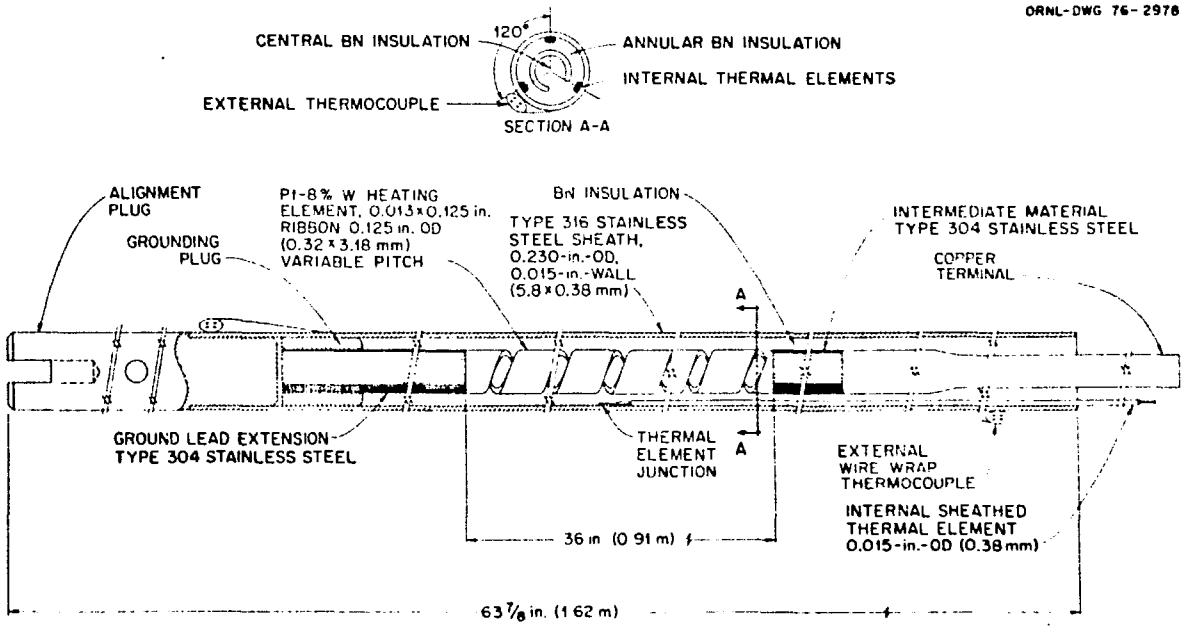


Fig. 2.4. Bundle 6A fuel pin simulator.

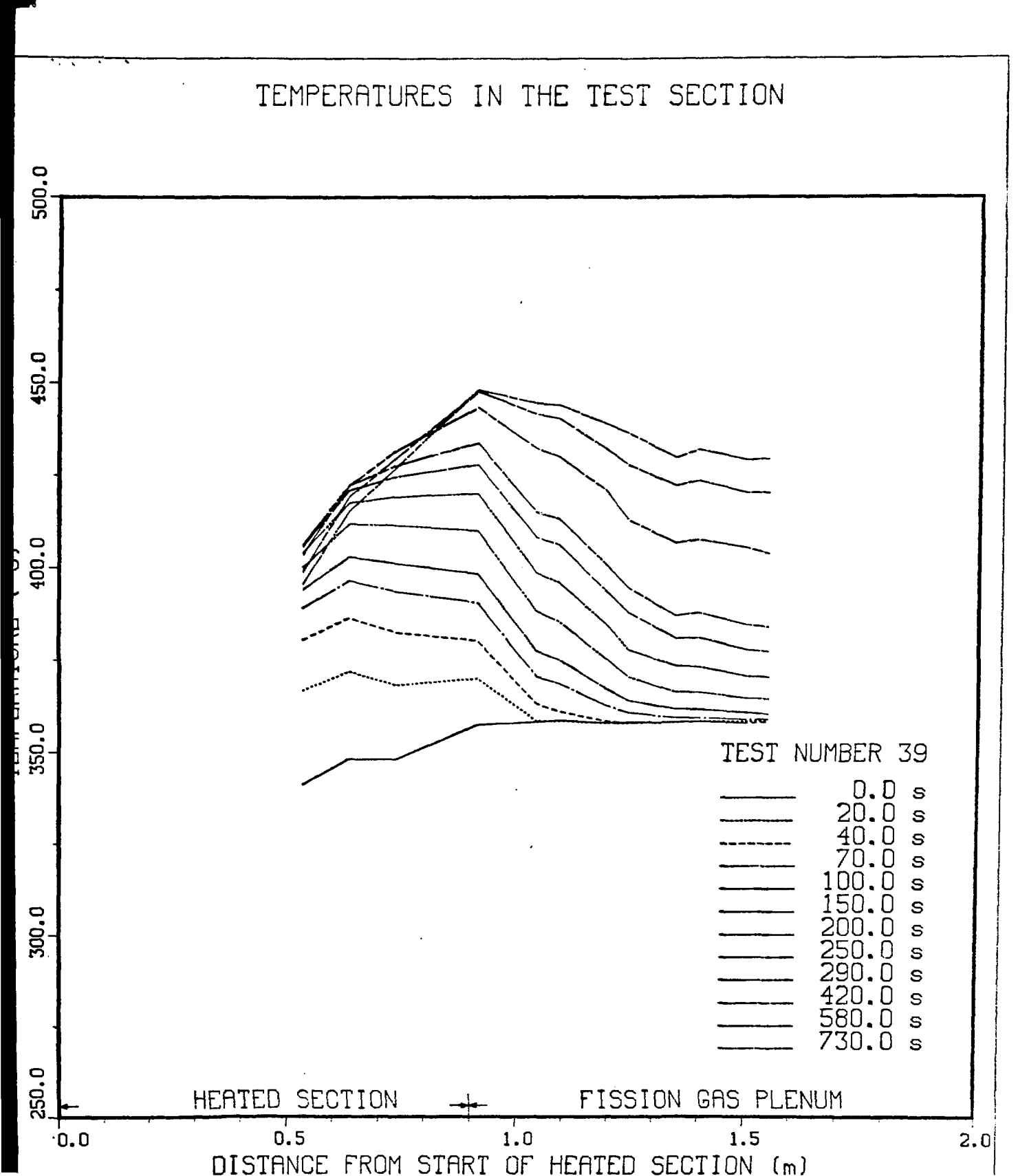
TEMPERATURES IN THE TEST SECTION
500.0
450.0
400.0
350.0
300.0
250.0
TEST NUMBER 39
0.0 s
20.0 s
40.0 s
70.0 s
100.0 s
150.0 s
200.0 s
250.0 s
290.0 s
420.0 s
580.0 s
730.0 s
HEATED SECTION
FISSION GAS PLENUM
0.0
0.5
1.0
1.5
2.0
DISTANCE FROM START OF HEATED SECTION (m)

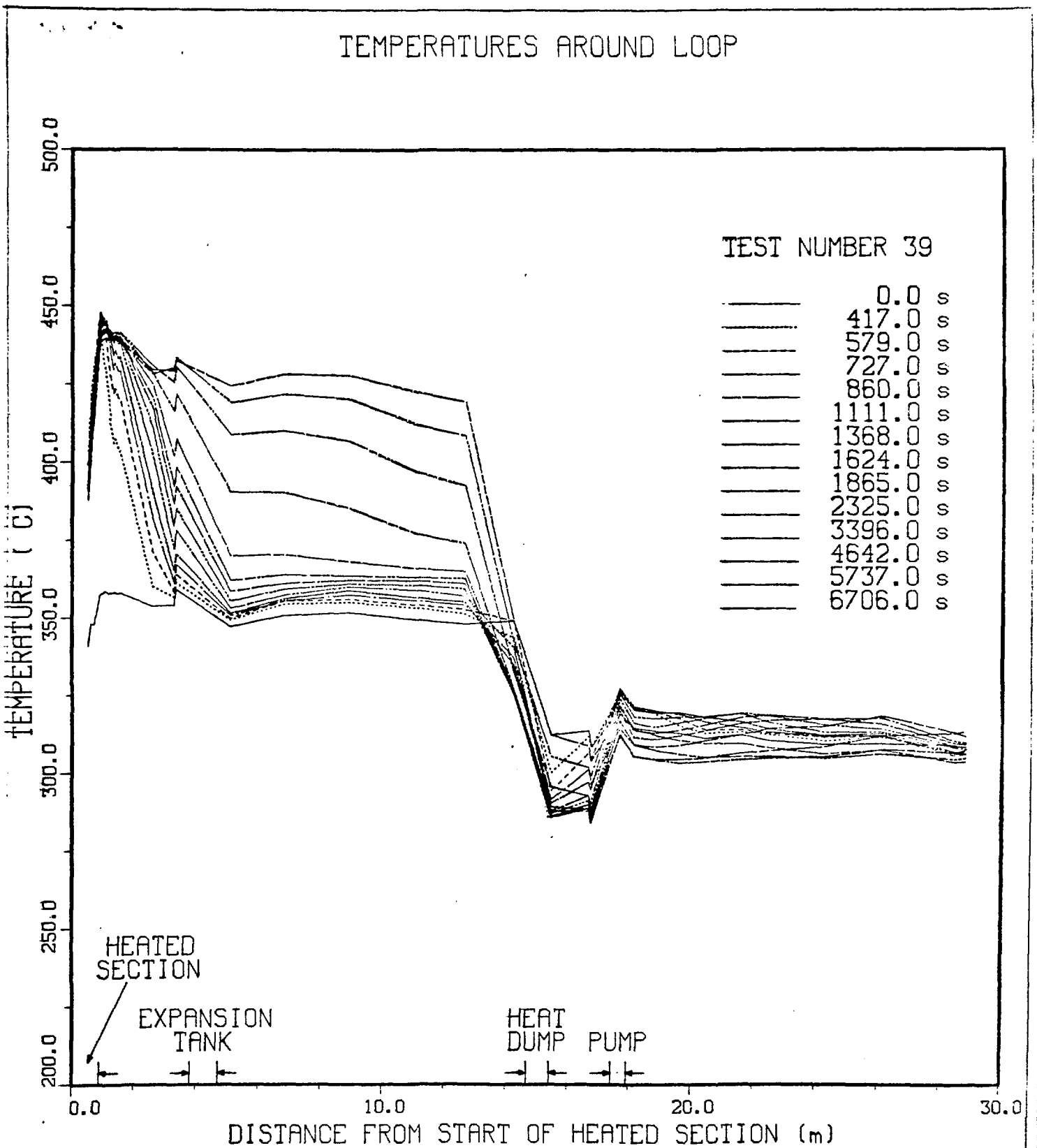


Fig. 3.2. Temperatures recorded around the THORS loop plotted at selected times during the transient, (THORS Bundle 6A, Test 39, initial low forced flow, bypass open).

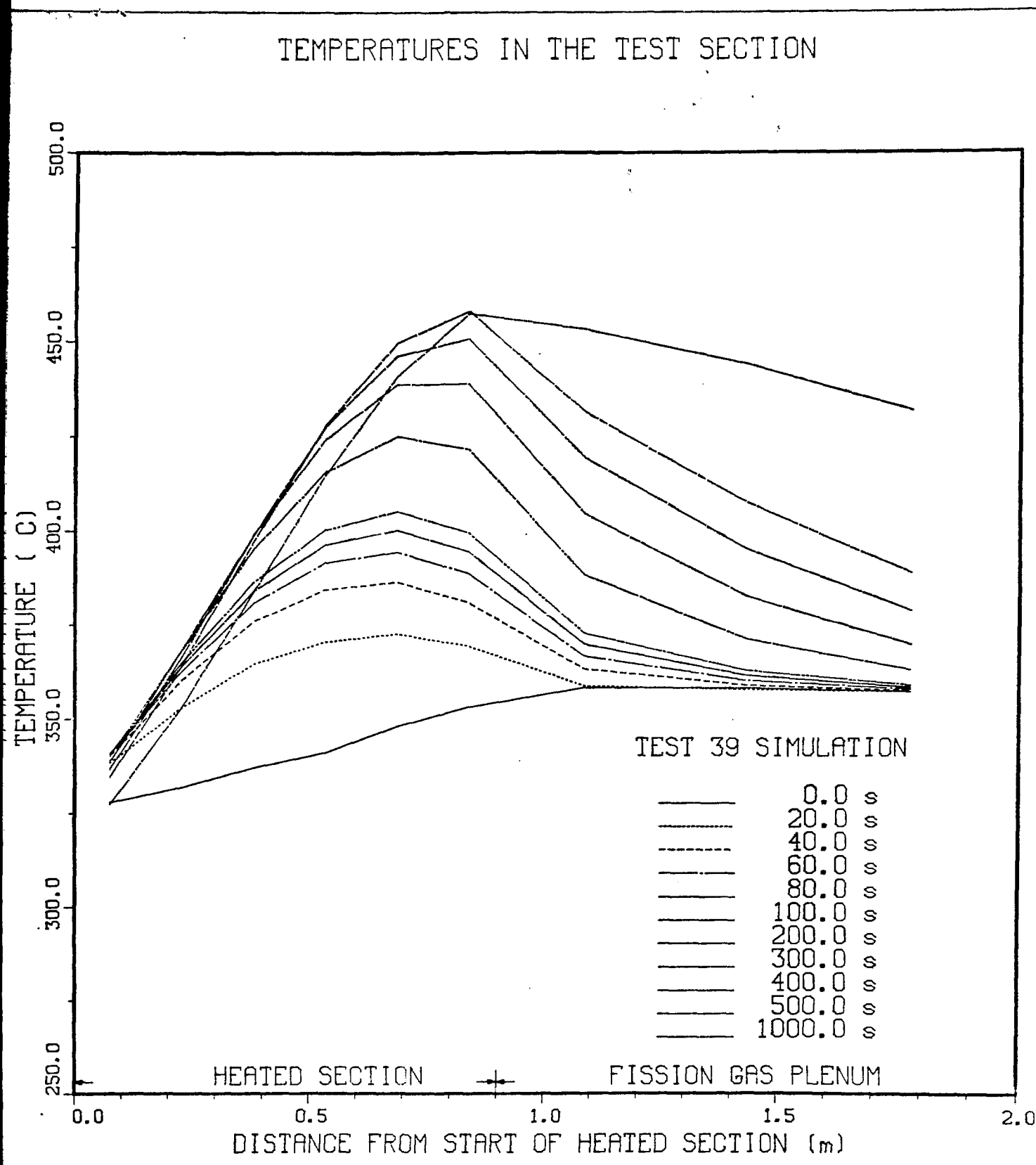


Fig. 4.1. Computed test section temperatures for various times early in the transient (LONAC simulation of THORS Bundle 6A, Test 39).

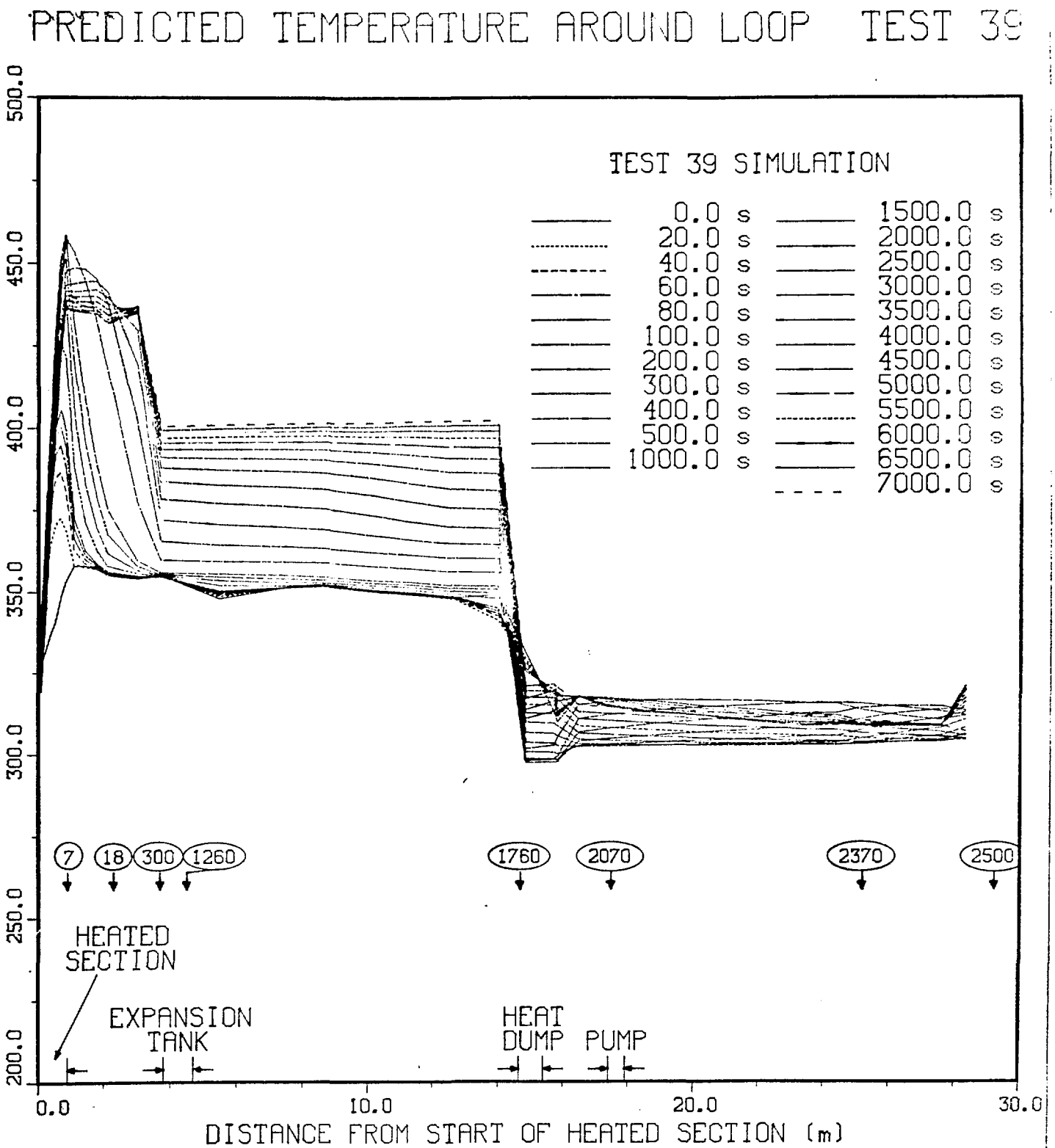


Fig. 4.2. Computed loop temperatures for various times during the transient, (LONAC simulation of THORS Bundle 6A, Test 39). Circled numbers indicate the time (sec) it would take a parcel of fluid leaving the beginning of the heated section at = 0 to reach the station indicated.

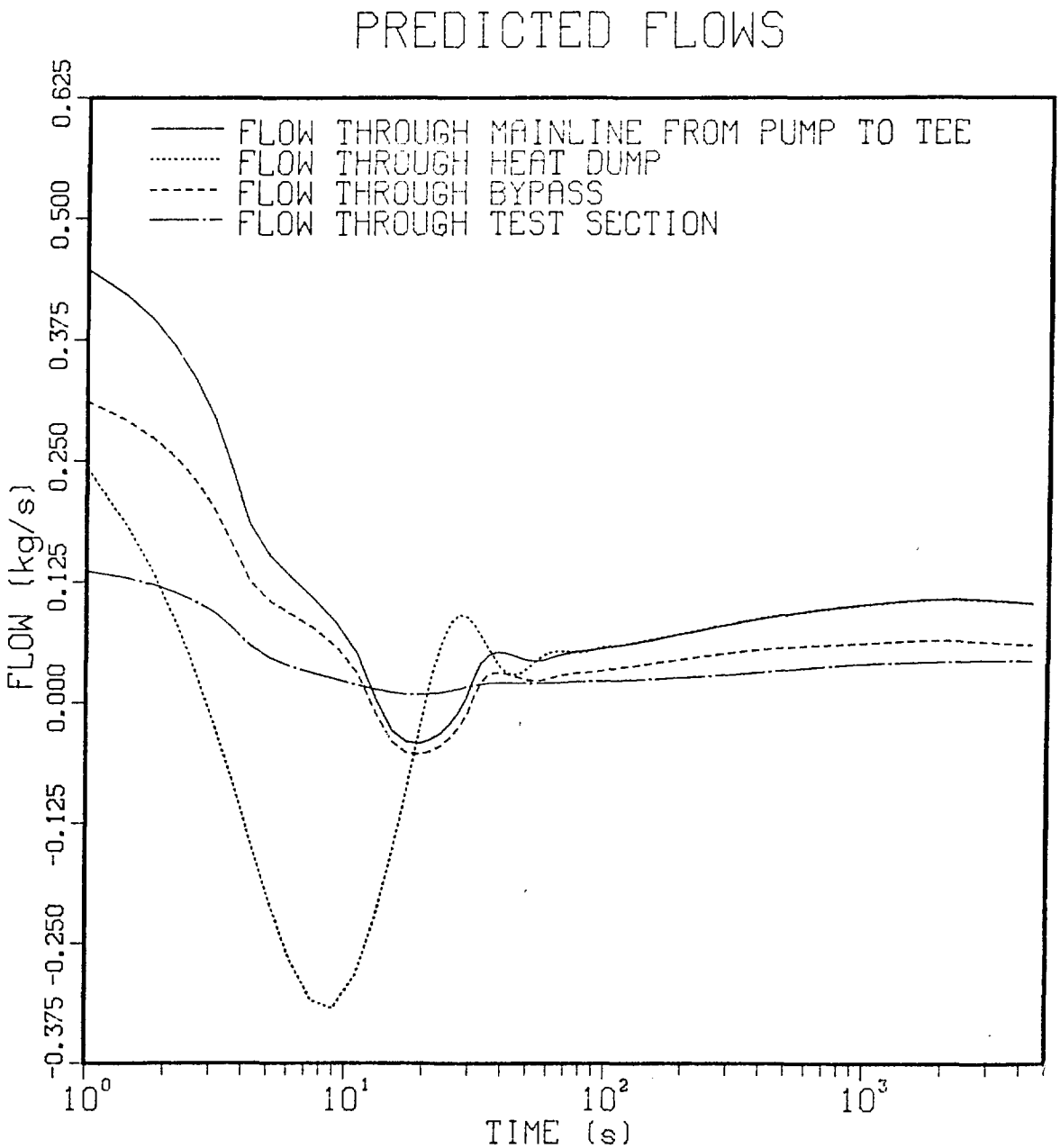


Fig. 4.3. Computed flows vs time (CONAC simulation of CWTF Bundle 6A, Test 39).

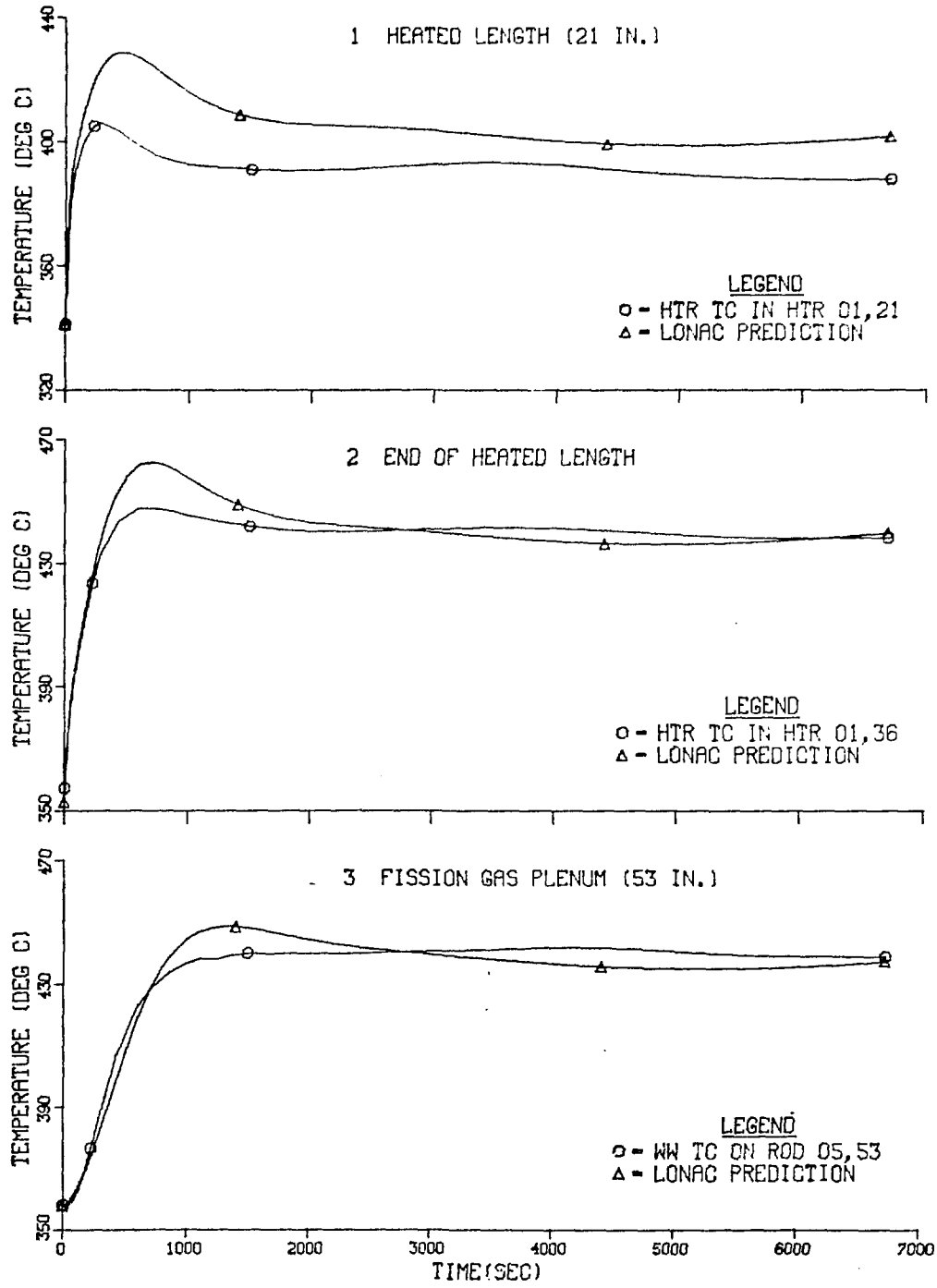




Fig. 4.4. Comparison of Test 39 thermocouple data with LONAC predictions at stations 1 through 3. Position of stations is indicated in Fig. 2.1.

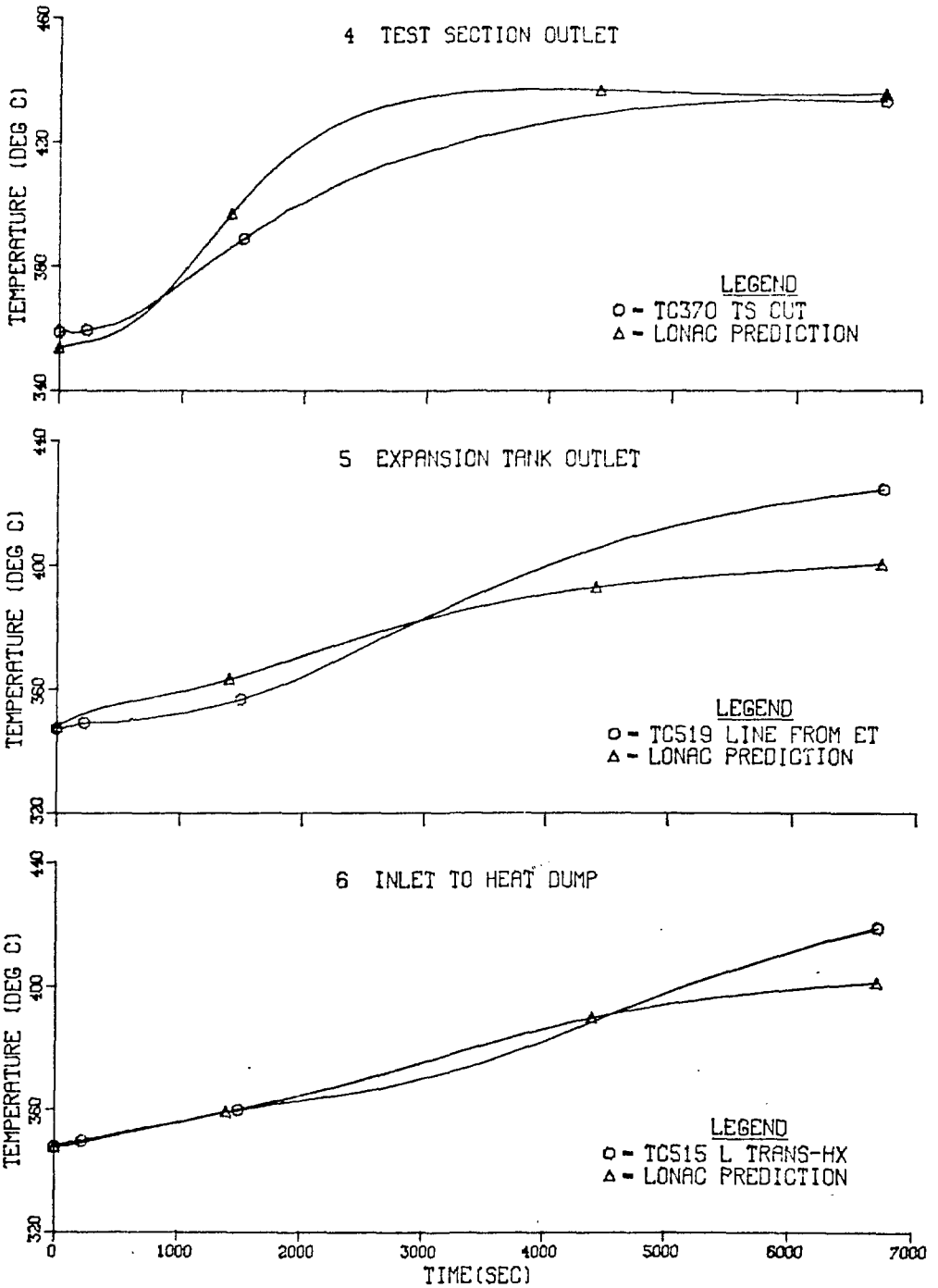


Fig. 4.5. Comparison of Test 39 thermocouple data with LONAC predictions at stations 4 through 6. Position of stations is indicated in Fig. 2.1.

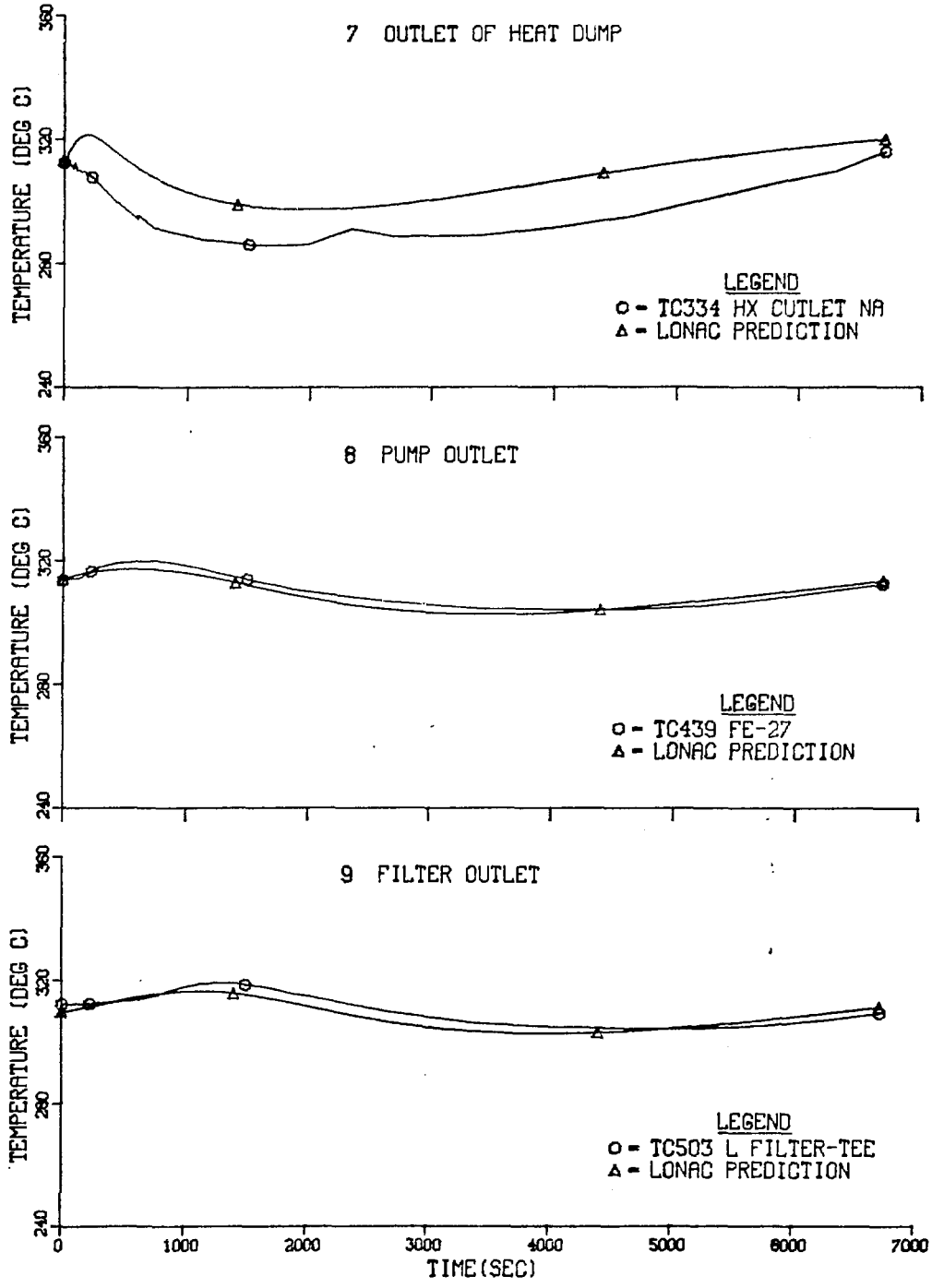




Fig. 4.6. Comparison of Test 39 thermocouple data with LONAC predictions at stations 7 through 9. Position of stations is indicated in Fig. 2.1.

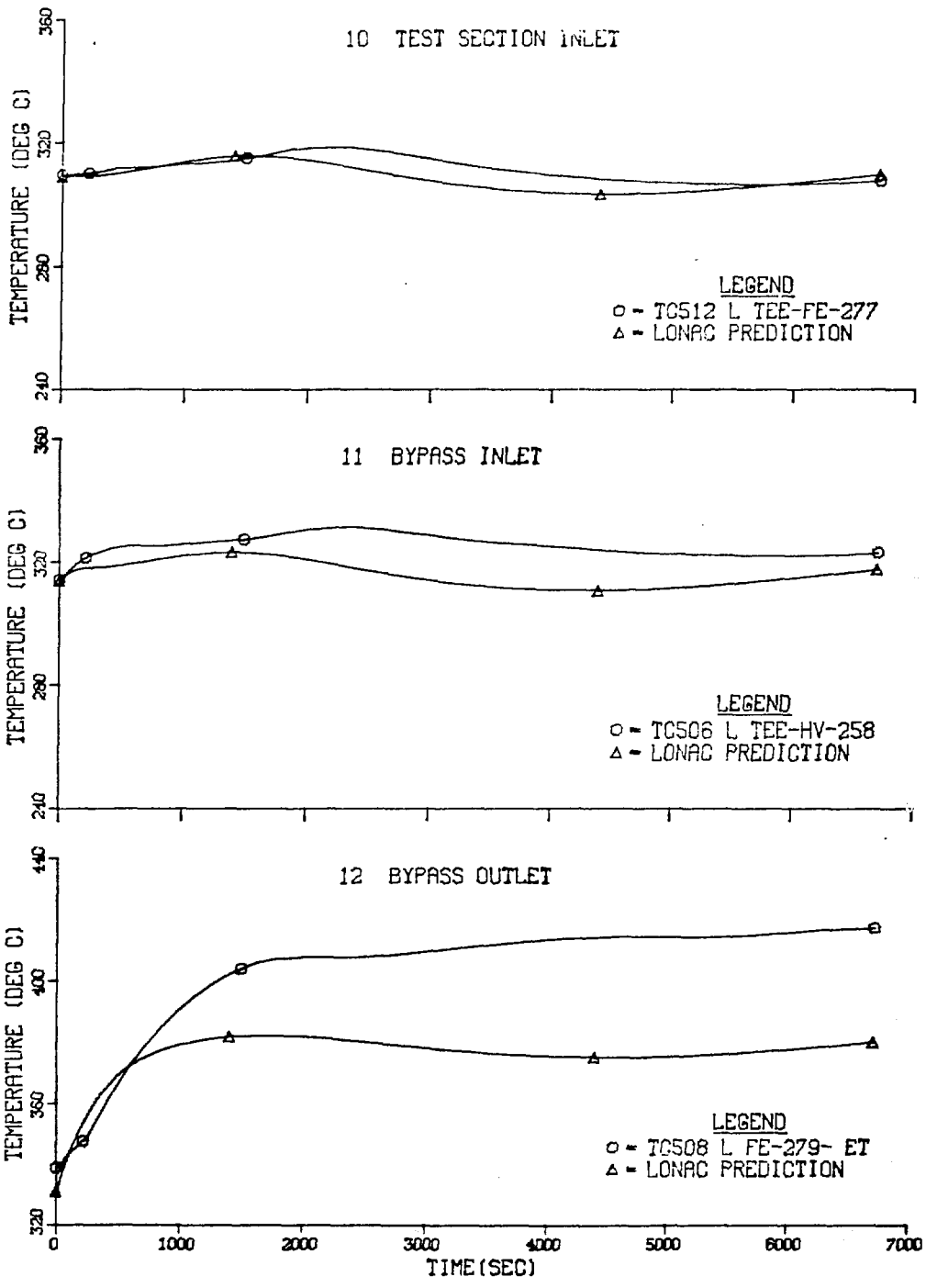


Fig. 4.7. Comparison of Test 39 thermocouple data with LONAC predictions at stations 10 through 12. Position of stations is indicated in Fig. 2.1.

CONF-790249--1

MASTER

# A PATHOGENIC MECHANISM IN LUNG FIBROSIS

Hanspeter Witschi, MD, Wanda M. Haschek, Ph.D., Kathleen R. Meyer, Ph.D., Robert L. Ullrich, Ph.D., and Walden E. Dalbey, Ph.D.

Biology Division
Oak Ridge National Laboratory
Oak Ridge, Tennessee 37830

---

Research sponsored by the Office of Health and Environmental Research, U. S. Department of Energy, under contract W-7504-eng-26 with the Union Carbide Corporation.

Synopsis

The purpose of the study was to examine whether an interaction between two agents causing alveolar epithelial damage would produce lung fibrosis. In mouse lung, intraperitoneal injection of the anti-oxidant butylated hydroxytoluene causes diffuse alveolar type I cell necrosis, followed by proliferation of type II alveolar cells. In animals exposed to 70% $O_2$ or 100-200 rad X-rays during the phase of type II cell proliferation following BHT, diffuse interstitial lung fibrosis developed within 2 weeks. Quantitative analysis of the lungs for hydroxyproline showed that the interaction between BHT and $O_2$ or X-rays was synergistic. If exposure to $O_2$ or X-rays was delayed until epithelial recovery was complete, no fibrosis was seen. Abnormally high levels of lung collagen persisted up to 6 months after one single treatment with BHT and 100 rad X-rays. A commonly seen form of chronic lung damage may thus be caused by an acute interaction between a bloodborne agent which damages the alveolar cell and a toxic inhalant or X rays, provided a critically ordered sequence of exposure is observed.

Pathogenetic features common to many forms of interstitial pulmonary fibrosis are a chronic alveolitis, changes in the cellular composition of the alveolar zone and derangement of the interstitial collagen. Fibrosis often appears to develop as a common sequel to injury when normal tissue repair fails to take place.[1] It may be precipitated and sustained by exposure to a single etiologic agent such as inhaled particles of silica or irradiation of the thorax. In other forms, such as idiopathic pulmonary fibrosis, the etiologic agent remains unknown. Recently we suggested that pulmonary fibrosis could develop following the interaction between an agent reaching the lung via the bloodstream and a toxic inhalant.[2] This speculation was based upon the following experimental observations.

In mice, the antioxidant butylated hydroxytoluene (BHT) causes widespread and uniform lung damage. Twenty-four hours after an intraperitoneal injection or oral administration of 200-400 mg/kg of BHT, diffuse necrosis of type I alveolar epithelial cells is seen throughout the lung. The initial damage is followed by a period of recovery. On days 2 and 3 after BHT there is intensive cell proliferation in lung, and total pulmonary DNA synthesis, measured by incorporation of labelled thymidine into pulmonary DNA, increases 10-15 fold.[3] In the early phase of recovery, most dividing cells are type II epithelial cells. From days 5 to 6 lesions develop in some capillary endothelial cells and endothelial cell proliferation follows. Interstitial cells appear not to be damaged, but also proliferate at this time. Six to 10 days after a single injection of BHT, the lungs regain a virtually

normal appearance. The morphologic sequence of events following BHT has been fully documented both by light- and electron microscopy.[4,5]

We subsequently examined the effects of $O_2$ exposure (60 to 100% for 10 to 24 hrs) upon lung cell division on different days after BHT. We found that $O_2$ inhibited cell division 2, 3 and 4 days after BHT, but no longer on days 5, 6 and 7.[6] Since the early phase after BHT is characterized by primarily division of type II alveolar cells, whereas interstitial cells divide on days 5 through 9 after BHT[4] we concluded that dividing epithelial cells might be more susceptible to the cytotoxic action of $O_2$ than dividing interstitial cells. Selective killing of epithelial cells by early oxygen exposure after BHT-induced lung injury could then allow excessive proliferation of interstitial cells and lead to the development of fibrosis. Experiments described in this paper were designed to test this hypothesis further.

## Methods

Young adult male BALB/c mice, weighing 20-25 g, were injected i.p. with a single dose of 400 mg/kg of BHT (3-5-di-tert-butyl-4-hydroxytoluene), dissolved in corn oil. Control animals received corn oil alone (0.1 ml/10g). Exposure to $O_2$ was performed in a plexiglass chamber, ventilated with a humidified mixture of $O_2$ and compressed air; the $O_2$ concentration was periodically monitored with an oxygen analyzer and kept within ±3% of the desired concentration. Local irradiation of the thorax was done with a GE Maxitron 300 X-ray machine operated at 300 kVp and 20 mA. The HVL was 1.29 cm Cu. The average dose rate was 265 rads/min.

Detailed experimental protocols are given in the results section.

At the end of the experiments, animals were anesthetized with sodium pentobarbital and exsanguinated via the abdominal aorta; the lungs were fixed in situ with 10% neutral buffered formalin injected through the trachea. Lung lobes were embedded in paraffin, sectioned at 3-4 μm and stained with hematoxylin and eosin, Masson's trichrome, van Gieson's and Snook's reticulin stains. Collagen was quantitated chemically in another group of mice by analyzing the lungs for hydroxyproline content. The lungs were perfused in situ with 0.9% NaCl, excised, lyophilized and hydrolyzed in 6 N HCl for 18 hrs at 107°C. Hydroxyproline was determined by a colorimetric assay[7] and all results were calculated as μg hydroxyproline per total lung. One-way analysis of variance was performed and a p value of $< 0.05$ was considered significant; comparisons of means were done by using Student's t-test. More details on methodological procedures have been given elsewhere.[2,8]

## Results

The first experiment was designed to examine the interaction between BHT and $O_2$. A group of mice received 400 mg/kg of BHT i.p. Half of the group was placed into 70% $O_2$ immediately after BHT and removed from the chamber 6 days later. The other half was kept in room air for 7 days and then placed in 70% $O_2$ for 6 days. Control groups were animals injected with corn oil, kept either in $O_2$ or in room air, and animals given 400 mg/kg of BHT and kept in room air. All animals were

killed for histopathologic analysis of the lung and determination of hydroxyproline two weeks after the BHT injection.

In oil treated control mice, total lung hydroxyproline varied between 200 and 230 μg/total lung, corresponding to 7.4-8.5 mg/g dry weight (Table 1). Exposure of oil-treated animals for 6 days to 70% $O_2$ alone was without any substantial effect upon total lung hydroxyproline. Administration of 400 mg/kg of BHT produced, within 2 weeks, a small increase in total pulmonary hydroxyproline. However, a much larger increase in total lung hydroxyproline, 150% over values found in the oil-treated control group, was found in animals given BHT and placed immediately for 6 days into 70% $O_2$. Since $O_2$ treatment alone had at best only a marginal effect and since BHT alone raised lung hydroxyproline only 50% above levels found in oil-treated controls the combined action of BHT and $O_2$ was not only additive, but synergistic. Histopathological examination showed that lungs from animals injected with oil and exposed to 70% $O_2$ were indistinguishable from the lungs of control animals kept in air. In animals treated with BHT, the acute mild pneumonitis seen 2-6 days after injection[4] was virtually resolved within 2 weeks and only focal alveolar wall hypercellularity and occasional intraalveolar macrophages remained (Figure 1). This was in sharp contrast to the lesions present in animals 2 weeks after treatment with BHT and immediate exposure for 6 days to $O_2$. Pulmonary architecture was severely disrupted due to cellular infiltration, primarily interstitial, and focal consolidation. There was a marked increase in interstitial cells or fibroblasts and in the amount of fibrillar material present within alveolar septa (Figure 2).

Special stains showed that the fibrillar material was positive for collagen and that there was a marked increase in reticulin fibers of variable length and thickness in the alveolar septa (Figure 3). The histopathological observations were thus in full agreement with the biochemical data.

On the other hand, when exposure to 70% $O_2$ was delayed until the 7th day after BHT, little fibrosis was observed histologically and the total lung hydroxyproline value was similar to the one found in animals treated with BHT alone (Table 1).

In the next experiment, animals were injected with BHT and placed immediately in 70% $O_2$ for 4 days. They were returned to room air and killed 2 weeks after BHT. Results in Table 2 show that a 4 day exposure to $O_2$ was almost as efficient as a 6 day exposure. If we waited until 3 days after BHT before placing the animals for 4 days into $O_2$, total pulmonary hydroxyproline content was still higher than in the lungs of animals treated with BHT alone, but somewhat lower than in the group placed immediately after BHT into $O_2$ (Table 2).

Another way to interfere with the epithelial recovery following BHT induced lung injury was to irradiate the lung with X-rays instead of exposing it to $O_2$. The data of this experiment are given in Table 3. Irradiation of control animals with 200 rad did not produce abnormal hydroxyproline accumulation in the lung within 2 weeks, and BHT treatment alone had only a slight effect. However, if 200 rad were delivered to the thorax one day after BHT, diffuse interstitial fibrosis developed within one to two weeks as determined by histological and

biochemical procedures. Delay of thorax irradiation until 6 days after BHT, on the other hand, was without any effect.

It was of interest to determine whether the increased levels of pulmonary hydroxyproline following the acute interaction between BHT and X-rays would persist for a prolonged time period. Data of such an experiment are given in Table 4. Significantly increased levels of total lung hydroxyproline were still present 6 months after an initial treatment with BHT and 100 rad given one day later. In contrast to the persistence of markedly elevated lung hydroxyproline levels, histological examination showed marked regression of lesions over the 24 week period. At two weeks there was marked interstitial pneumonitis (Figure 4) with focal consolidation, fibroblastic proliferation and an increase in reticulin fibers on Snook's reticulin stain. Consolidation was most frequently subpleural and associated with partial parenchymal collapse adjacent to ectacic bronchioles. By 24 weeks the inflammatory component of the lesion had virtually disappeared leaving behind slightly thickened and hypercellular alveolar septa with indistinct borders (Figure 5). Persistence of the increased number of reticulin fibers could be detected with Snook's reticulin stain. Focal subpleural consolidation and parenchymal collapse also persisted.

## Discussion

The data presented in this paper show that it is possible to produce an abnormal and persistent accumulation of collagen in mouse lung by combining two treatments: first, administration of BHT, a

bloodborne agent which causes diffuse and uniform necrosis of the type I alveolar epithelial cells, followed by a treatment (exposure to 70% $O_2$ or low doses of X-rays) which inhibits or prevents cell division in lung. The developping lesions are indicative of diffuse interstitial fibrosis. Preliminary ultrastructural observations suggest that this model has many features in common with the Hammon-Rich syndrome in man (Brody, A., personal communication).

Quantitative determination of lung hydroxyproline shows that BHT alone causes a significant increase in collagen, whereas neither 70% $O_2$ nor 200 rad X-rays are sufficient to produce fibrosis. If BHT is combined with either $O_2$ exposure or thorax irradiation the total amount of hydroxyproline found in lung now exceeds by far the amount which accumulates after BHT alone. The two insults to the lung have thus a synergistic effect. However, synergism is only seen if a strict temporal relationship between the two exposures is maintained. Oxygen exposure or thorax irradiation must occur within the first few days following BHT injection. If $O_2$ exposure or thorax irradiation is delayed for 6 days there is no abnormal accumulation of lung collagen and no histopathological evidence of interstitial fibrosis. There is also no fibrosis if $O_2$ or X-rays are administered prior to BHT.[2,8]

The mechanism underlying this interaction between BHT and $O_2$ or X-rays in causing lung fibrosis has not been fully elucidated. At present, we explain our findings as follows: following the initial lung damage, there is first a proliferation of epithelial cells. If $O_2$ or X-rays interfere with this phase of epithelial cell proliferation

which is essential for reestablishment of a normal alveolar surface, the interstitial cell population could begin to grow comparatively uninhibited. In support of this hypothesis is the observation made in another experimental model: if an excised trachea is stripped of its epithelium and implanted subcutaneously into a syngeneic host, the tracheal lumen will become obliterated with connective tissue within a very short time. However, if isolated epithelial cells are reintroduced into the tracheal lumen, reepithelizsation follows and the trachea remains open.[9] In trachea, fibroblasts grow thus excessively in the absence of an intact epithelium. It is tempting to speculate that the proliferation of interstitial cells in the alveolar zone is controlled, directly or indirectly, by the continuous presence of an intact epithelial layer.

It will be important to examine in future studies whether we can produce a similar interaction between agents other than BHT and $O_2$ or X-rays, and then come to a general conclusion about the pathogenetic principle underlying the development of at least some forms of lung fibrosis. Diffuse damage to the alveolar zone may be caused by many toxic inhalants or by several bloodborne agents.[10] It is also conceivable that the same or other agents might interfere with epithelial recovery following the initial injury. A commonly seen form of chronic lung damage might thus be caused by an acute synergistic interaction between two agents, provided a critically ordered sequence of exposure takes place.

There are two specific clinical situations where it is conceivable that the development of fibrotic lung changes might be enhanced by

a synergism similar to the one seen in our animal studies. Adequate treatment of critically ill patients often requires $O_2$ therapy. It is however often difficult to decide on the concentration of $O_2$ and the duration of treatment which will not cause lung damage. Many patients will suffer from adult respiratory distress syndrome and whether the lesion develops can often not be predicted.[11] Since trauma, shock, fatty embolism and many drugs can cause acute alveolar damage[12] it is possible that development of pulmonary complications during $O_2$ therapy is determined by the presence and severity of initial lung damage rather than by the $O_2$ treatment. If this can be substantiated, it will become necessary to devise appropriate diagnostic tests which would allow detection of alveolar epithelial cell damage so that patients at risk can be identified.

Lung fibrosis can also develop within a few weeks in patients treated with irradiation to the thorax and given concomittantly antineoplastic agents such as bleomycin, cyclophosphamide, actinomycin D or others.[13] Cytotoxic agents are known to cause acute alveolar cell death. It is feasible that the accelerated development of radiation-induced lung fibrosis is caused by a mechanism similar to the one found in the study of BHT and X-ray interaction. Based on these findings, timing between drug administration and chest irradiation might be an important factor in determining whether excessive fibrosis develops.

References


1. Fulmer, JD, Crystal, RG: The biochemical basis of pulmonary function. In The Biochemical Basis of Pulmonary Function, Crystal, RG ed. New York, Marcel Dekker, 1976.

2. Haschek, WM, Witschi, HP: Pulmonary fibrosis - a possible mechanism. Toxicol. Appl. Pharmacol. (in press).

3. Witschi, HP, Saheb, W: Stimulation of DNA synthesis in mouse lung following intraperitoneal injection of butylated hydroxytoluene. Proc. Soc. Exp. Biol. Med. 147:690-693, 1974.

4. Adamson, IYR, Bowden, DH, Côté, MG, Witschi, HP: Lung injury induced by butylated hydroxytoluene. Cytodynamic and biochemical studies in mice. Lab Invest. 36:26-32, 1977.

5. Hirai, KI, Witschi, HP, Côté, MG: Electron microscopy of butylated hydroxytoluene-induced lung damage. Exp. Mol. Pathol. 27:295-308, 1977.

6. Witschi, HP, Côté, MG: Inhibition of butylated hydroxytoluene induced mouse lung cell division by oxygen: time-effect and dose-effect relationships. Chem. Biol. Interactions 19:279-284, 1977.

7. Stegemann, H., Stalder, K: Determination of hydroxyproline. Clin. Chim. Acta 18:267-273, 1967.

8. Haschek, WM, Meyer, KR, Ullrich, RL, Witschi, HP: Potentiation of chemically induced lung fibrosis by thorax irradiation. Int. J. Radiat. Oncol. Biol. Phy. (in press).

9. Terzaghi, M, Nettesheim, P, Williams, ML: Repopulation of denuded tracheal grafts with normal, preneoplastic and neoplastic epithelial cell populations. Cancer Res. 38:4546-4553, 1978.

10. Witschi, HP, Côté, MG: Primary pulmonary responses to toxic agents. CRC Crit. Rev. Toxicol. 5:23-66, 1977.

11. Pratt, PC: Pathology of adult respiratory distress syndrome. In The Lung, Structure, Function and Disease. Thurlbeck, WM, and Abell, MR ed., Baltimore, MD, Williams and Wilkins, 1978.

12. Katzenstein, ALA, Bloor, CM, Liebow, AA: Diffuse alveolar damage - the role of oxygen, shock and related factors. Am. J. Pathol. 85:210-228, 1976.

13. Gross, H: Pulmonary effects of radiation therapy. Ann. Intern. Med. 86:81-92, 1977.

Figure 1.

Lungs from mice injected i.p. with 400 mg/kg BHT, kept in air, and killed 2 weeks after BHT. Hypercellularity of the alveolar septa and occasional intraalveolar macrophages are present. H & E x 200.

Figure 2.

Lungs from mice injected i.p. with 400 mg/kg BHT, immediately exposed to 70% oxygen for 6 days, and killed 2 weeks after BHT. Disruption of normal parenchymal architecture is due to cellular infiltration and consolidation. H & E X 200.

Figure 3.

Lungs from mice injected i.p. with 400 mg/kg BHT, immediately exposed to 70% oxygen for 6 days, and killed 2 weeks after BHT. Large numbers of reticulin fibers of varying thickness are present in alvolar septa and area of consolidation. Snook's reticulin stain X 500.

Figure 4.

Lungs from mice injected i.p. with 400 mg/kg BHT, irradiated with 100 rad X-ray one day later, and killed 2 weeks after BHT. Interstitial pneumonitis characterized by hypercellularity and thickening of alveolar walls is present. H & E X 250.

Figure 5.

Lungs from mice injected i.p. with 400 mg/kg BHT, irradiated with 100 rad X-ray one day later, and killed 24 weeks after BHT. Alveolar walls are slightly thickened and hypercellular with indistinct borders. H & E X 250.

Table 1: Total lung hydroxyproline in mice exposed to 70% $O_2$ following BHT[a]

| Treatment[b] | Hydroxyproline per lung (μg) | |
|---|---|---|
| | Oxygen exposure on days 1-6 after BHT[c] | Oxygen exposure on days 7-12 after BHT[d] |
| Corn oil + air | 206 ± 5 | 226 ± 8 |
| Corn oil + 70% $O_2$ | 228 ± 4[e] | 220 ± 3 |
| BHT + air | 296 ± 21[e] | 307 ± 19[e] |
| BHT + 70% $O_2$ | 539 ± 19[e,f] | 321 ± 14[e] |

[a]Data from reference 8; values are means ± SE from 8-10 animals/group

[b]Male mice received BHT (400 mg/kg) i.p. or corn oil (0.1 ml/10g) i.p. and were killed 2 weeks later.

[c]Exposure to 70% $O_2$ begun immediately after BHT injection.

[d]Exposure to 70% $O_2$ begun 7 days after BHT injection.

[e]$p < 0.05$ compared to animals injected with corn oil and kept in air.

[f]$p < 0.05$ compared to animals injected with BHT and kept in air.

Table 2: Total lung hydroxyproline in animals exposed to 70% $O_2$ on different days after BHT

| Treatment[a] | Hydroxyproline per lung (μg)[b] |
|---|---|
| BHT and 70% $O_2$ on days 1, 2, 3, 4 | 421 ± 18[c,d] |
| BHT and 70% $O_2$ on days 3, 4, 5, 6 | 341 ± 12[c] |
| BHT and air | 283 ± 10 |

[a]Male mice injected with 400 mg/kg of BHT and kept in 70% $O_2$ as indicated, otherwise in air; all animals killed 2 weeks after BHT.

[b]Mean ± SEM; from 10 animals per group.

[c]$p < 0.05$ compared to animals injected with BHT and kept in air

[d]$p < 0.05$ compared to animals injected with BHT and exposed to $O_2$ on days 3-6.

Table 3: Total lung hydroxyproline in animals irradiated with 200 rad X-rays on different days after BHT[a]

| Treatment[b] | Hydroxyproline per lung (µg) | |
|---|---|---|
| | Irradiated 1 day after BHT[c] | Irradiated 6 days after BHT[d] |
| Corn oil + sham irradiation | 178 ± 3 | 219 ± 4 |
| Corn oil + 200 rad | 184 ± 5 | 215 ± 6 |
| BHT + sham irradiation | 259 ± 6[e] | 295 ± 16 |
| BHT + 200 rad | 371 ± 26[e,f] | 284 ± 9 |

[a]Data from reference 9; values are means ± SE from 10 animals/group

[b]Male mice received BHT (400 mg/kg) i.p. or corn oil (0.1 ml/10g) i.p. and were killed 2 weeks later.

[c]200 rad to the thorax 1 day after BHT.

[d]200 rad to the thorax 6 days after BHT.

[e]$p < 0.05$ compared to animals injected with oil and sham irradiated.

[f]$p < 0.05$ compared to animals injected with BHT and sham irradidated.

Table 4: Total lung hydroxyproline in animals irradiated with 100 rad X-rays 1 day after BHT[a]

| Weeks after BHT | Hydroxyproline per lung (µg) | | | |
|---|---|---|---|---|
| | BHT + 100 rad | BHT + Sham | Corn oil + 100 rad | Corn oil + Sham |
| 2 | 371 ± 15(7)[b] | 287 ± 7(8) | 213 ± 6(8) | 223 ± 6(8) |
| 6 | 358 ± 21(6)[b] | 282 ± 5(8) | 233 ± 6(7) | 233 ± 10(8) |
| 12 | 404 ± 28(7)[b] | 325 ± 10(8) | 257 ± 9(8) | 278 ± 3(7) |
| 24 | 387 ± 27(7)[b] | 319 ± 12(8) | 280 ± 6(8) | 248 ± 8(8) |

[a]Male mice received BHT (400 mg/kg) or corn oil (0.1 ml/10g) i.p. and were irradiated with 100 rad to the thorax or sham irradiated 1 day later. The animals were killed 2, 6, 12 or 24 weeks after BHT.

[b]$p < 0.05$ compared to animals treated with BHT and sham irradiated.

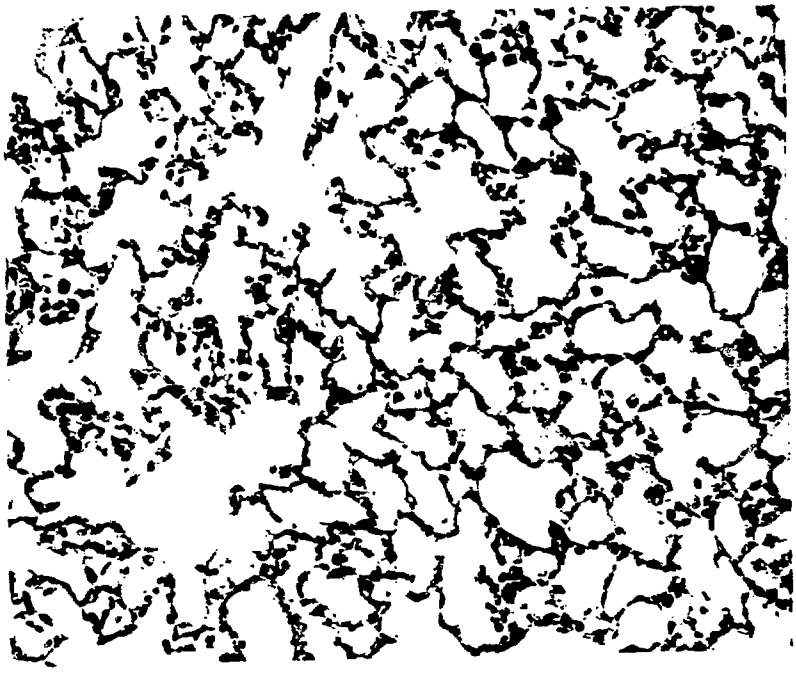

fig 1

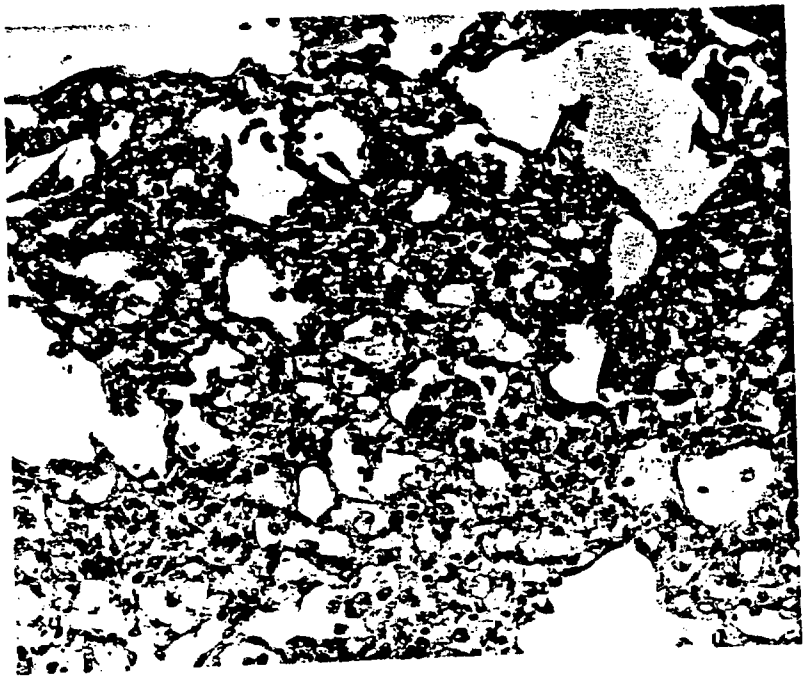

fig 2

fig 3

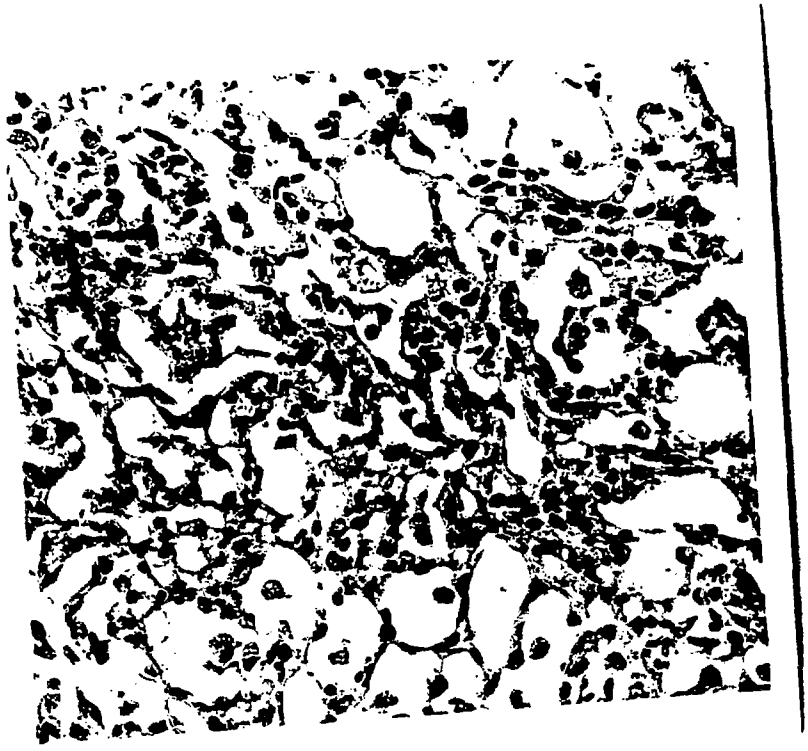

fig 4

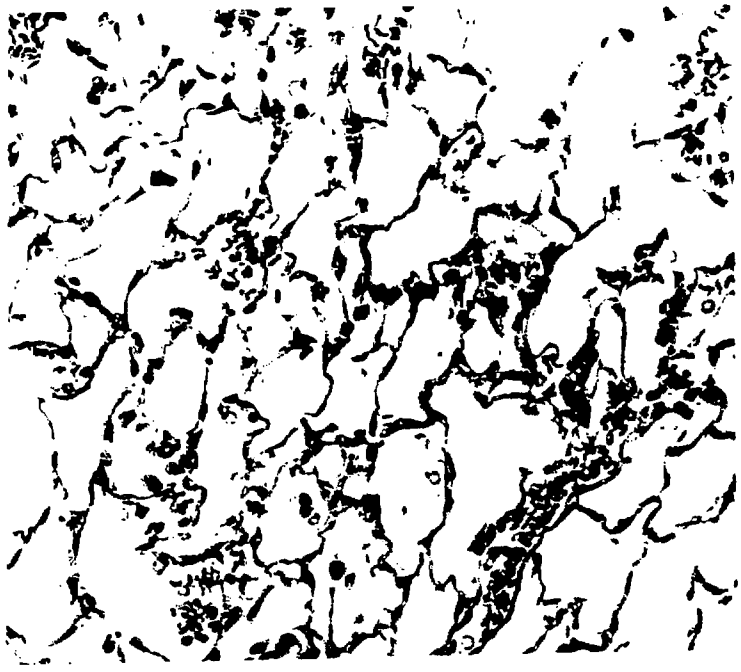

fig 5